A Continuum Mechanical Approach to Model Leaf Growth

A Thesis

submitted to
Indian Institute of Science Education and Research Pune
in partial fulfillment of the requirements for the
BS-MS Dual Degree Programme

by

Sukrit Jaiswal

Indian Institute of Science Education and Research Pune
Dr. Homi Bhabha Road,
Pashan, Pune 411008, INDIA.

April, 2023

Supervisor: Prof Dr Miltos Tsiantis

Certificate

This is to certify that this dissertation entitled A Continuum Mechanical Approach to Model Leaf Growthtowards the partial fulfilment of the BS-MS dual degree programme at the Indian Institute of Science Education and Research, Pune represents study/work carried out by Sukrit Jaiswal at Indian Institute of Science Education and Research under the supervision of Prof Dr Miltos Tsiantis, Professor, Department of Comparative Genetics and Diversity, subgroup Plant Development and Diversity , during the academic year 2022-2023.

Prof Dr Miltos Tsiantis

Committee:

Prof Dr Miltos Tsiantis

Prof Apratim Chatterji

Declaration

I hereby declare that the matter embodied in the report entitled A Continuum Mechanical Approach to Model Leaf Growth are the results of the work carried out by me at the Department of Comparative Genetics and Diversity, subgroup Plant Development and Diversity, Indian Institute of Science Education and Research, Pune, under the supervision of Prof Dr Miltos Tsiantis and the same has not been submitted elsewhere for any other degree.

Sukrit Jaiswal

Acknowledgments

My heartfelt thanks go to each member of my loving family for their unwavering love, encouragement, and support throughout my academic journey. Their constant support has been instrumental in my success.

I would like to express my deepest gratitude to my supervisors Dr Soeren Strauss and Dr Gabriella Mosca for their guidance, patience, and unwavering support throughout the entire research process. Their expertise and invaluable feedback were crucial in shaping the direction of this thesis and the research conducted.

I would also like to thank Prof Miltos Tsiantis and Prof Apratim Chatterjee for their insightful suggestions, which greatly improved the quality of this thesis and allowing me to work with them.

I would also like to extend my gratitude to my friends and colleagues in the institute for their support, encouragement, and their stimulating discussions, which provided me with new ideas and perspectives. Shoutout to Rachita, Jeroen, Ziliang, Alessandro, Nora, XinMin, Jisha, Sara, Manas and Gaurav.

Special thanks to Ravish Mehta and Prateek Lamoria, who generously gave their time, listened to my woes and shared their experiences, while helping me stay positive, without which this research would not have been possible.

Finally, I would like to thank IISER Pune and Max Planck Institute for Plant Breeding Research for providing me with the opportunity to pursue my master's degree, and for their resources and facilities, which were essential in completing this thesis.

Abstract

Understanding how organ shapes are produced and the causes of their variety is a major problem in biology. The difficulty in solving the issue lies in the fact that the final form frequently relies on mechanical constraints from nearby areas rather than being a direct readout of locally specified characteristics. We can distinguish between specified growth, which is the growth that would happen if each region grew separately from its neighbors (i.e., in mechanical isolation), and resultant growth, which is the growth that is observed when the mechanical constraints of adjacent regions are taken into account. (i.e. mechanically connected tissue). Here, we use numerical and computational modeling using continuum mechanics (for finding the compatible configuration) to try to find a solution to this problem. In order to describe the mechanical characteristics that underpin the growth of leaf cells, we create models of leaf evolution at various degrees of abstraction.

Contents

List of Figures

Chapter 1

Introduction

1.1 Leaf Morphogenesis and heteroblasty

Leaf morphogenesis is a complex process that involves the regulation and coordination of various genetic and environmental factors. This process leads to the development of leaves, which are essential organs in plants. Leaves are responsible for photosynthesis, gas exchange, and transpiration, and play a crucial role in plant growth, development, and reproduction.

The process of leaf morphogenesis starts with the emergence of a small group of undifferentiated cells from the shoot apical meristem called the leaf primordium. [1] The leaf primordium forms at the site where the leaf will grow and develops into a mature leaf through various stages. The stages in leaf maturation include cell division, cell elongation, and cell differentiation.

The genetic factors involved in leaf morphogenesis [2] interact to create a unique and diverse range of leaf shapes and sizes among different plant species. The study of leaf morphology is beneficial in understanding plant evolution, adaptation, and ecology. Furthermore, understanding the mechanisms that regulate leaf development is essential for improving crop yields, developing new plant-based products and technologies, and advancing our knowledge of plant biology and ecology [3].

Researchers use Arabidopsis in plant biology research as a model organism to study leaf devel-

opment and heteroblasty because the plant is easy to grow and manipulate in the laboratory, there is a complete sequence of genomes avaialble, and because its small size and transparent tissues make it possible to observe and analyze leaf development in detail. Studies of Arabidopsis have provided valuable insights into the genetic and molecular mechanisms that control leaf heteroblasty in plants [4].

Leaf heteroblasty [5] refers to the phenomenon where a plant's leaves undergo changes in shape, size, and structure as they develop. This results in leaves of different ages appearing significantly different from each other. This process is thought to be an adaptive strategy that allows plants to optimize their growth and development in response to changing environmental conditions, such as changes in light, water availability, or temperature. By producing leaves of different shapes and sizes, plants can adjust their photosynthetic and transpiration rates, as well as their ability to capture and retain water and nutrients, according to their needs at different stages of growth [6].

In Arabidopsis, leaf heteroblasty is evident in the transition from the embryonic leaves to the true leaves. The embryonic leaves are relatively simple, undifferentiated structures, while the true leaves show a more complex and differentiated structure. The first few true leaves produced by Arabidopsis are small and round. As the plant continues to grow, subsequent leaves become larger and more elongated, with pronounced serrations 1.1.

Figure 1.1: The different leaves of the Arabidopsis Thaliana Wildtype Col-0 Plant (image courtesy XinMin Li, shown with permission). ScaleBar = 1 cm

1.2 Computational Modelling

Computational modelling is a powerful tool for studying complex biological processes such as leaf morphogenesis. Recently in years, computational models have been developed to simulate various aspects of leaf development, including the growth and differentiation of leaf cells, the effects of environmental factors on leaf morphology, and the interaction between genetic and environmental factors. [7]

One approach to modelling leaf development is to use agent-based models (ABMs) [8]. ABMs simulate the behaviour of individual agents (such as cells) and their interactions with each other and their environment. ABMs can be used to model various aspects of leaf development, such as the growth and division of cells, the regulation of cell differentiation, and the impact of environmental factors on cell behaviour. ABMs have been used to study the effects of light on leaf development, the role of auxin in leaf patterning, and the influence of mechanical forces on leaf shape. These models do not accurately account for plant cell behavior and as are symplactically growing and attached to each other via a lamella, while ABM assume an attraction potential which can lead to changes in connectivity.

Another approach to modelling leaf development is to use partial differential equation models. Such models describe the behaviour of a system as a function of space and time. [9] PDE models which are used to simulate the growth and differentiation of cells in a developing leaf can also model the effects of environmental factors such as temperature and humidity on leaf morphology. PDE models have been used to study the growth patterns of leaves, the role of hormone gradients in leaf patterning, and the impact of environmental factors on leaf growth and development. Some models are centred on pattern emergence and some models connect pattern of morphogens to leaf evolving shapes.

In addition to ABMs and PDE models, other types of computational models have been developed to simulate leaf development. For example, Boolean models [10] use a set of logical rules to describe the behaviour of a system. Boolean models have been used to study the genetic regulation of leaf development and the interaction between different genetic pathways. Furthermore, machine learning algorithms have been used to analyse large datasets of leaf morphology and to identify patterns and relationships between different morphological traits.

Computational modelling of leaf development is a rapidly growing field, with new models and algorithms being developed and refined every year. These models have the potential to provide new insights into the mechanisms that regulate leaf development and to aid in the development of new crops with improved leaf traits. Additionally, computational modelling can help to identify new targets for genetic engineering and to predict the effects of environmental factors on plant growth and development.

1.3 Resultant vs Specified Growth

Computational leaf modeling involves the use of computer models to simulate the growth and development of plant leaves. In few models, growth is typically represented as a combination of cell division, elongation, and differentiation.
One common approach to modeling leaf growth was based on the idealised assumption that the leaf grows through the addition of new cells [11]. As these cells divide and elongate, the leaf expands in size and shape. However this has proven to be false. In some models [12], the division and elongation of cells are governed by specific growth rules or algorithms.

There has been much theoretical and experimental research on the patterns of gene activity and how they are established in animals and plants, but little is known about how these patterns relate to tissue development and deformation. This is a difficult problem since an organism's final form is controlled by mechanical limitations from its surroundings as well as by local features. For instance, the wavy edge that results when the growth rate at the margin of a leaf is higher than that at the center develops through the interplay between growth patterns and mechanical restrictions rather than being specifically stated [13, 14]. In such circumstances, it is possible to distinguish between stipulated growth (which would take place in mechanical isolation) and resulting growth (seen in a tissue that is mechanically coupled).

Growth can be divided into two categories: specified and resultant. Specified growth is the growth that would happen if a canvas element developed independently from other elements, whereas resultant growth is directly observable by tracking or clonal analysis [15, 16]. The growth that results is a result of specific growth in several places interacting with one another through related tissue. Figure 1.2 gives an illustration of this. Panel (A) shows a square tissue that has been fragmented into little tiles in its basic form. Panel (B) displays how each tile would be impacted separately

if it were not connected to its neighbors if we applied a radially growing field of locally isotropic growth. It soon becomes clear that these tiles cannot be deformed further to form a continuous tissue without gaps. Panel (C) shows the final tissue after integrating local growth with mechanical constraints.

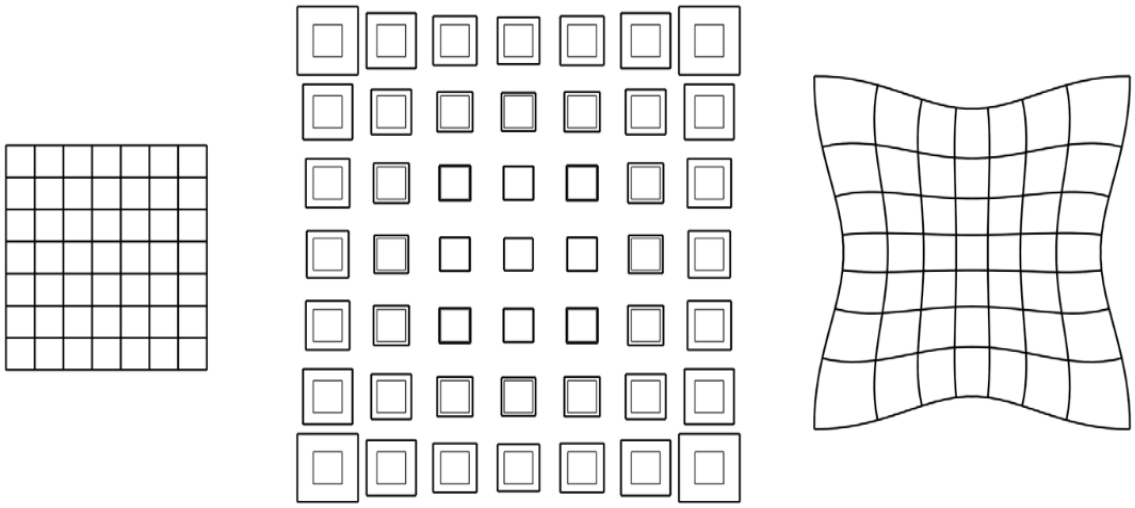

Figure 1.2: (A) The starting point. (B) An exploded view shows the expansion of each tile, with the initial sizes overlay in gray. (C) The minimal-energy form resulting from the continuity restriction (image adapted from [9])

Tracking tissue deformations over time may be used to measure resultant growth, but knowing how genes control specific development is necessary to appreciate the mechanisms that cause resultant growth. Genes only need to regulate the local growth rate when a defined growth is isotropic. However, it is possible for defined growth to be anisotropic in many cases, necessitating genetic regulation of both growth rates and orientations.

1.4 Work in this thesis

Our work is conducted within the MorphoMechanX framework, which utilizes newly developed FEM code by Mosca [1]. Specifically, we have created a 2D FEM membrane model that incorporates various technological and physical advancements, enabling us to generate diverse leaf shapes.

The goal of our research is to create a comprehensive model that integrates biomechanics, which can be utilized by both biologists and modellers for the analysis of leaf growth, development, and patterning. We have placed significant emphasis on incorporating various morphogens and examining their interactions, in order to meet the diverse needs of future research. Additionally, we have developed a documented LeafGarden that features a wide range of relevant leaf shapes generated by our model, and have compared these shapes with previous works to verify the accuracy of our model.

The problem statement of this thesis is stated in Chapter 1, which provides an introduction to modeling and leaf development.
The foundation of elasticity theory, which forms the core of MorphoMechanX, is introduced in Chapter 2 along with a brief overview of continuum mechanics theory.
For triangular linear membrane elements subject to the effects of growth for hyperelastic material laws, a finite element method (FEM) model is implemented, as described in Chapter 3. This model-specific program now has a number of additional capabilities that are described.
Different models that the program imitated are discussed in Chapter 4 along with how it aids in our comprehension of the growth that results from these models. It provides an implementation of a model for leaf development. The amount and the direction of growth can be regulated by morphogens in combination with a mechanical feedback mechanism. The model allowed to show how, under simple and biologically justifiable hypotheses, one can reproduce leaf shapes and growth data at a qualitative level.

Chapter 2

Finite Strain Theory

2.1 Fundamentals

In the context of solid mechanics, growth can be modeled using the theory of finite strain, which considers the deformation of a material as a continuous change in its shape and size. In this framework, growth is viewed as a combination of deformation and volume changes.
Finite strain theory is based on the concept of strain, which describes the comparative change in shape and size of a material as it undergoes deformation. Strain can be expressed mathematically as a tensor that relates the change in length and orientation of a material to its initial state.

When applied to growth, finite strain theory allows for the modeling of changes in shape and size that occur as a result of cell division, elongation, and differentiation. In this framework, the deformation of a material is captured by a deformation gradient tensor, which captures the local changes in shape and orientation of the material due to growth. The volume changes associated with growth can be incorporated into the model by introducing a growth tensor, which describes the rate of growth and its direction at every point in the material.

We present the ideas of continuum mechanics [17, 18, 19], which serves as the foundation for non-linear elasticity and deals with large-scale deformations caused by rotations and/or stresses. The continuum configurations in this instance that are undeformed and deformed differ greatly from one another. They serve as the model and software's building blocks, hence they are crucial.

2.1.1 Configuration

At a specific moment in time t, there exists a continuum body B with a particle P that is located within it. This body is embedded within three-dimensional Euclidean space.

A reference frame is established at a stationary origin O, consisting of right-handed, rectangular coordinate axes with orthonormal basis vectors e_a. As the continuum body B moves through space over time, it passes through a continuous sequence of configurations, represented by $\Omega_o, ..., \Omega$. Each particle P of the continuum body B corresponds to a geometrical point that exists within the regions $\Omega_o, ..., \Omega$. These regions denote the configurations of B at a given time t. It is important to note that B can occupy an infinite number of configurations within space.

At each moment in time, the geometrical areas are uniquely specified, and the fixed reference configuration, denoted by the symbol Ω_o, corresponds to a fixed reference time. Dynamics studies usually do have the initial configuration selected as the reference configuration. The start-up configuration is at the same time as the reference time. At time $t = 0$, the particle P is identified by its position vector (or referential position), or X, with regard to a fixed origin, O.

The continuum body B's configuration at time t is known as the current (or deformed) configuration at a later time $t > 0$. At periods $t = 0$ and $t > 0$, the typical position X of the reference configuration is connected to a point x of the present configuration occupied by particle P.

2.1.2 Motion

We make the assumption that the function $X = K_o(P,t)$ establishes a one-one relationship between the point $X \in \Omega_o$ that B occupies at time t = 0 and a particle $P \in B$. We also assume that the function K operates on B to generate the region Ω at time t. The position $x = K(P,t)$ can be expressed symbolically and in index notation as:

$$\begin{aligned} x &= K[K_o^{-1}(X,t)] = \chi(X,t) \\ x_a &= \chi_a(X_1, X_2, X_3, t) \end{aligned} \tag{2.1}$$

for all $X \in \Omega_o$ and for all times t.

Here, χ is a vector field that represents the motion of body B and provides the location x corresponding to each X for all fixed t. The motion χ converts locations x in the present configuration Ω from points X from Ω_o. We presume that χ has continuous spatial and temporal derivatives. A typical particle P's sequential locations in space are described by equation 2.1, and these positions combine to create a curve we refer to as the particle P's trajectory. We believe that the motion χ is invertible. A body's form, position, and orientation often change as a result of motion. Deformable continuum bodies are those that can alter their shape.

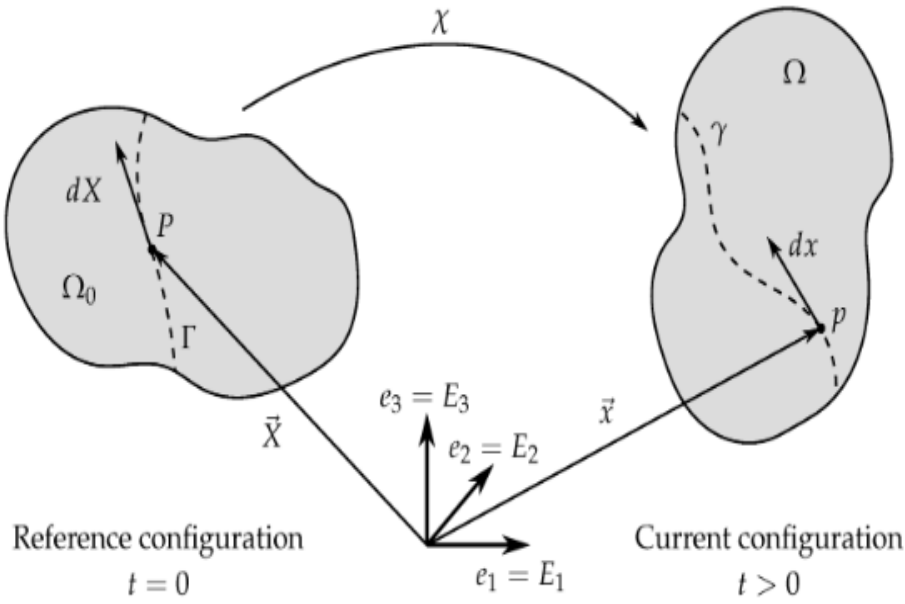

Figure 2.1: A continuum body's configuration and motion (image adapted from [20])

2.1.3 Material and spatial descriptions

According to 2.1, the material (or referential) description describes motion (or other qualities) in relation to the material coordinates (X_1, X_2, X_3). Such a description focuses on and follows the movement of a particle. It's also known as the Lagrangian description.

The Eulerian description, describes motion (or other qualities) in terms of the spatial coordinates (x_1, x_2, and x_3). As such, this description concentrates on a specific location in space and examines what transpires there throughout time.

2.1.4 Displacement Field

The vector field denoting a typical particle's displacement field is described as

$$U(X,t) = x(X,t) - X \tag{2.2}$$

that connects the particle's position X in its undeformed configuration to its correspondng position x in the deformed configuration. All particles and the displacement field U are subject to this relationship. U is a function of the referential point X and time t when describing the material description (Lagrangian form) of the displacement field. The two descriptions are connected by the motion $x = \chi(X,t)$ as

$$U(X,t) = U[\chi^{-1}(x,t),t] = u(x,t) \tag{2.3}$$

Any particle moves the equal amount and in the same direction for a rigid-body translation. Therefore, the displacement field in this scenario is independent of X and might be a function of time t.

2.1.5 Material Derivatives

The idea of material fields is introduced, with the independent variables for material fields being referential location X with material coordinates X_A and time t. $F = F(X,t)$ denotes a smooth and continuous material field of some amount connected with motion χ.

A continuous material field $F(X,t)$ has its material time derivative indicated as $DF(X,t)/Dt$ or a dot function, i.e. $\dot{F}(X,t)$

$$\dot{F}(X,t) = \frac{DF(X,t)}{Dt} = \left(\frac{\partial F(X,t)}{\partial t}\right)_X \tag{2.4}$$

Deriving F with regard to reference location X at a specified time t, the material field $F(X,t)$'s material gradient, denoted as Grad $F(X,t)$, is

$$\text{Grad } F(X,t) = \frac{\partial F(X,t)}{\partial X} \tag{2.5}$$

The material divergence of F (Div F) and curl of F (Curl F) are differential operators characterize values relative to the reference configuration.

2.2 Deformation Gradient

The goal of this section is to study the deformation of a continuum body occurring when it moves from the reference configuration Ω_o to the current configuration Ω.

2.2.1 Deformation gradient

Understanding the mapping between a location in the reference configuration Ω_o, indicated by X, and a position in the current configuration Ω, denoted by x, is necessary to examine how curves and tangent vectors deform.

In order to create the equivalent spatial curve $x = \gamma(\xi, t)$ at time t for a material curve $X = \Gamma(\xi)$ in the reference configuration, which is linked to the continuum body, a specific motion χ is applied.

$$x = \gamma(\xi, t) = \chi(\Gamma(\xi), t) \tag{2.6}$$

Both the material and spatial tangent vectors to the material curve are represented by the letters dX and dx, respectively. These vector elements are known as the "spatial line element" in the current and the "material line element" in the reference configurations respectively.

$$dx = \frac{\partial \gamma(\xi, t)}{\partial \xi} d\xi \tag{2.7}$$

$$dX = \frac{\partial \Gamma(\xi, t)}{\partial \xi} d\xi \tag{2.8}$$

The deformation gradient tensor F is a vital component of nonlinear continuum mechanics, describes the connection between the material and spatial tangent vectors. The tensor F is a tensor with elements arranged in two different ways, with the first index representing spatial coordinates and the second index representing the material coordinates. It utilizes the transformation rule to

convert material tangent vectors to spatial tangent vectors through the following equation:

$$dx = F(X,t)dX \tag{2.9}$$

$$\text{where} \qquad F(X,t) = \frac{\partial \chi(X,t)}{\partial X} = \text{Grad } x(X,t) \tag{2.10}$$

When the tensor F does not rely on the spatial coordinates, which is equivalent to an affine motion, it is said to be homogeneous. The tensor F is often inhomogeneous because it depends on the material coordinates X. When we consider the case of a rigid body translation, F = I, with I being the identity tensor.

2.2.2 Nanson's formula

As we are aware, the reference configuration's points, curves, and tangent vectors, represented by X, Γ, and dX, respectively, map onto the current configuration's points, curves, and tangent vectors, denoted by x, γ, and dx, respectively. The current configuration counterpart of any differential vector is mapped by the deformation gradient tensor F given as

$$dx = F(X,t)dX \tag{2.11}$$

A unit vector N which is normal to an infinitesimal undeformed surface element dS does not, however, transfer through F to a unit vector n which is normal to the corresponding infinitesimal deformed surface element ds. This is demonstrated by the fact that at time t, the difference in volume compared in the reference configuration with the current configuration, given by

$$dv = J(X,t)dV \tag{2.12}$$

with

$$J(X,t) = \det F(X,t) > 0 \tag{2.13}$$

J is the volume ratio, also known as the Jacobian determinant. Here, the terms material (undeformed) and spatial (deformed) volume elements dV and dv respectively denote the infinitesimal volume elements as defined in the respective configurations. We have $dV = dX_1 dX_2 dX_3$ and $dv = dx_1 dx_2 dx_3$ assuming that the volume is a continuous function of continuum particles.

We consider a material line element called dX that maps to dx when a motion χ occurs. In the

current configuration, the infinitesimal volume element may be written as $ds \cdot dx = JdS \cdot dX$, where $ds = dsn$ signify vector element with small area specified in the current configuration and likewise $dS = dSN$ in the reference configuration.

The equation may be revised to read

$$(F^T ds - JdS) \cdot dX = 0 \tag{2.14}$$

This is true for all possible material line components dX. We then come across that

$$ds = JF^{-T} dS \tag{2.15}$$

which illustrates the relationship between the vector elements of the infinitesimally small areas ds and dS. This connection is known as Nanson's formula.

2.3 Strain Tensors

The deformation gradient is an essential kinematic tensor in finite deformation kinematics, as we discovered in the previous section. It illustrates how material elements change while they are in motion. The objective of this section is to identify these modifications as second-order strain tensors associated with the actual configuration and the reference configuration. It's vital to remember that strains are based on a notion developed to simplify studies, unlike displacements, which are measured.

2.3.1 Material strain tensors

We measure how a motion affects the length between two nearby locations in area Ω_o, X and Y. The term "neighboring" refers to the proximity of X to Y. In terms of the material line element,

$$dX = Y - X \tag{2.16}$$

where $d\varepsilon$ stands for the material length, the geometry in the reference configuration is stated.

$$dX = d\varepsilon a_o \tag{2.17}$$

$$d\varepsilon = |Y - X| \tag{2.18}$$

The material line element's direction at X is described by the unit vector a_o, which is

$$a_o = \frac{Y - X}{|Y - X|} \tag{2.19}$$

where $|a_o| = 1$ at the referential location X. $d\varepsilon^2$ is the dot product of dX and itself.

$$dX \cdot dX = d\varepsilon a_o \cdot d\varepsilon a_o = d\varepsilon^2 \tag{2.20}$$

During certain motions of regions Ω, the two adjacent points X and Y are changed into their new locations, $x = \chi(X,t)$ and $y = \chi(Y,t)$. The relative velocity $y - x$ can be roughly calculated using the linear term $F(Y - X)$, where F is the deformation gradient.

We introduce the stretch ratio λ_{a_o} in the direction of the unit vector a_o, which has a length $\lambda = |\lambda_{a_o}|$. The length of a spatial line element is derived as $\lambda d\varepsilon$ initially in the direction of a_o where $d\varepsilon$ is the material length.

We define the right Cauchy-Green tensor C, which is symmetric and positive definite for each $X \in \Omega_o$, as an essential strain measure in material coordinates

$$C = F^T F \tag{2.21}$$

Only the direction of a_o at a location $X \in \Omega_o$ and the second-order tensor C are required to determine the stretch of a fiber.

Using definition (2.13) and equations (2.21), we can determine that the determinant of the tensor C, denoted as det C, is equal to the square of the determinant of the tensor F, denoted as det F, which is greater than zero, i.e.,

$$\det C = (\det F)^2 = J^2 > 0 \tag{2.22}$$

We define the change in squared lengths to measure further strain, i.e., $(\lambda d\varepsilon)^2 - d\varepsilon^2$. Using (2.20), we can rewrite this expression as

$$\frac{1}{2}[(\lambda d\varepsilon)^2 - d\varepsilon^2] = \frac{1}{2}[(d\varepsilon a_o) \cdot F^T F(d\varepsilon a_o) - d\varepsilon^2] = dX \cdot EdX \tag{2.23}$$

where

$$E = \frac{1}{2}(F^T F - I) \tag{2.24}$$

The 1/2 is a normalization factor in the linear theory. This equation describes a strain measure in the direction of a_o at point X in Ω_o. E is the Green-Lagrange Strain Tensor. It can be deduced from (2.24) that $E = E^T$ since I and C are symmetric.

2.4 Balance Principles

In all branches of continuum mechanics, the fundamental principles of balance of momentum, conservation of mass [17, 18], and balance of energy remain valid. They must always be satisfied and are applicable to any particular material.

2.4.1 Balance of Mechanical Energy

For the coming analyses, we assume a dynamical process with a motion $x = \chi(x,t)$ that deforms any area Ω_o to Ω, and a symmetric Cauchy stress tensor $\sigma = \sigma(x,t)$. The material mass density $\rho_o(X)$ and the current mass density $\rho(x,t)$ are continuous scalar fields that describe mass. The former is independent of time and connected to the body's reference configuration, whereas the latter changes with time and is reliant on a body location. Utilizing the limit of increasing mass of incremental volume elements, which is expressed in

$$\rho_o(X) = lim_{\Delta V(\Omega_o)\to 0} \frac{\Delta m(\Omega_o)}{\Delta v(\Omega_o)} \tag{2.25}$$

$$\rho(x,t) = lim_{\Delta V(\Omega)\to 0} \frac{\Delta m(\Omega)}{\Delta v(\Omega)} \tag{2.26}$$

where Δm denotes a continuous function of increase in mass of a volume element shown as ΔV in the reference and and as Δv in the current configuration.

External mechanical power and kinetic energy

We look at a collection of particles that share a bound area Ω with a boundary surface $\partial\Omega$ and we first describe quantities in terms of material coordinates. The power input performed by the system of forces (T,B) on an area Ω at time t is specified as the external mechanical power, abbreviated as P_{ext}

$$P_{ext}(t) = \int_{\partial\Omega} T \cdot V ds + \int_{\Omega} B \cdot V dV \tag{2.27}$$

Here, $T \cdot V$ and $B \cdot V$ are scalar quantities that provide the external mechanical power per unit reference surface S and reference volume V and the material velocity field denoted by $V = \dot{X}$, and $T \cdot V$ and $B \cdot V$ are scalar quantities that provide the external mechanical power per unit reference surface S and reference volume V, respectively. Dimensionally, P_{ext} is power as it equates work per time.

As an extension of Newtonian mechanics to continuum mechanics, the definition of the kinetic energy K of a continuum body which occupies a space at time t is as follows:

$$K(t) = \int_{\Omega} \frac{1}{2} \rho_o V^2 dV = \int_{\Omega} \frac{1}{2} \rho_o V_a V_a dV \tag{2.28}$$

The reaction of an area Ω to the stress field at time t is described by the stress power which is the rate of internal mechanical work indicated by P_{int}:

$$\begin{aligned} P_{int}(t) &= \int_{\Omega} \sigma : d dV = \int_{\Omega} tr(\sigma^T d) dV \\ P_{int}(t) &= \int_{\Omega} \sigma_{ab} d_{ab} dV \end{aligned} \tag{2.29}$$

The stress power P_{int} is zero because the rate of deformation tensor d is zero for a rigid-body motion.

Mechanical energy balance in material description

Establishing the stress power P_{int}, the kinetic energy K, and the external mechanical power P_{ext} is necessary to define the mechanical energy balance in terms of material coordinates.

Thus, the external mechanical power P_{ext} is obtained as

$$P_{ext}(t) = \int_{\partial\Omega_o} T \cdot V dS + \int_{\Omega_o} B \cdot V dV \tag{2.30}$$

The kinetic energy K is given as

$$K(t) = \int_{\Omega_o} \frac{1}{2}\rho V^2 dV = \int_{\Omega_o} \frac{1}{2}\rho V \cdot V dV = \int_{\Omega_o} \frac{1}{2}\rho V_a V_a dV \tag{2.31}$$

The first Piola-Kirchhoff stress tensor P can be used to express the rate of internal mechanical work (stress-power) P_{int}. We see that

$$P_{int}(t) = \int_{\Omega} \sigma : d dv = \int_{\Omega} \sigma : (\dot{F}F^{-1}) dv = \int_{\Omega} \sigma F^{-T} : \dot{F} dv = \int_{\Omega_o} J\sigma F^{-T} : \dot{F} dV \tag{2.32}$$

The symbol : stands for second order tensor double contraction, in Cartesian coordinates is

$$A : B = A_{ij} B_{ij} \tag{2.33}$$

With the Piola transformation, we can obtain the equivalence for the rate of internal mechanical work

$$P_{int}(t) = \int_{\Omega_o} P : \dot{F} dV = \int_{\Omega_o} tr(P^T \dot{F}) dV \tag{2.34}$$

We can express the mechanical energy balance in the material description equivalently to

$$\frac{D}{Dt} \int_{\Omega_o} \left(\frac{1}{2}\rho_o V^2 \right) dV + \int_{\Omega_o} P : \dot{F} dV = \int_{\partial\Omega_o} T \cdot V dS + \int_{\Omega_o} B \cdot V dV \tag{2.35}$$

With respect to the reference volume, using the internal energy defined as $e = e(x,t)$, we can express this equation as a function of internal energy. With $dv = JdV$ and motion $x = \chi(X,t)$,the internal energy can be written

$$E(t) = \int_{\Omega} e_c(x,t) dv = E(t) = \int_{\Omega_o} e_c(\chi(X,t),t) J(X,t) dV = \int_{\Omega_o} e(X,t) dV \tag{2.36}$$

with the necessary change of variables

$$e_c(x,t) J(X,t) = e(X,t) \tag{2.37}$$

The total energy in the material description can be expressed as

$$\int_{\Omega_o} \left(\frac{1}{2} \rho_o V^2 + e \right) dV \tag{2.38}$$

using the expressions for kinetic energy K and internal energy E. By using the equivalence of equations, and the total energy, the equation is obtained

$$\frac{D}{Dt} \int_{\Omega_o} \left(\frac{1}{2} \rho_o V^2 + e \right) dV = \int_{\partial \Omega_o} T \cdot V dS + \int_{\Omega_o} B \cdot V dV \tag{2.39}$$

which can be derived from the balance of energy directly requiring the transformation

$$\int_{\Omega_o} P : \dot{F} dV = \frac{D}{Dt} \int_{\Omega_o} e dV \tag{2.40}$$

Conservative system

The functions Π_{ext} and Π_{int} are scalar-valued and represent the potential energy of external loading and total strain energy of a body, respectively. The sum of these functions is called the total potential energy or energy functional Π of the mechanical system, which is expressed as the sum of Π_{ext} and Π_{int}, i.e.

$$\Pi(t) = \Pi_{ext}(t) + \Pi_{int}(t) \tag{2.41}$$

A conservative mechanical system is considered when the external mechanical power P_{ext} and internal mechanical power P_{int} are related as follows:

$$P_{ext}(t) = -\frac{D\Pi_{ext}}{Dt} = -\dot{\Pi}_{ext}(t) \tag{2.42}$$

$$P_{int}(t) = \frac{D\Pi_{int}}{Dt} = \dot{\Pi}_{int}(t) \tag{2.43}$$

$$\Pi_{int}(t) = \int_{\Omega_o} \psi dV \tag{2.44}$$

Here, ψ represents the strain energy function defined per unit volume. Assuming certain conditions, the sum of potential energy Π and kinetic energy K must be conserved for the balance of mechanical energy during a dynamic process, i.e.

$$\Pi_{ext}(t) + \Pi_{int}(t) + K(t) = const \tag{2.45}$$

Chapter 3

Concept and Modelling of Growth

Growth occurs in biological systems through a variety of physical and chemical factors. Computational techniques like finite element analysis can be used to model growth (see chapter 1.2). In these models, the deformed configuration portrays the system's development through time, whereas the reference configuration depicts the system's undeformed condition.

The reference configuration is subjected to localized minor deformations to imitate growth. Without putting any pressure or stress on the system, these deformations lead it to change its size and shape. The compatibility condition, a fundamental mechanics concept that calls for the deformation to be continuous and smooth over the whole system [9], is not naturally satisfied, however, because the deformation is local.

To satisfy the compatibility requirement, the growth deformation must be combined with an elastic deformation. The elastic deformation allows the system to accommodate the growth-induced changes without violating the compatibility requirement.

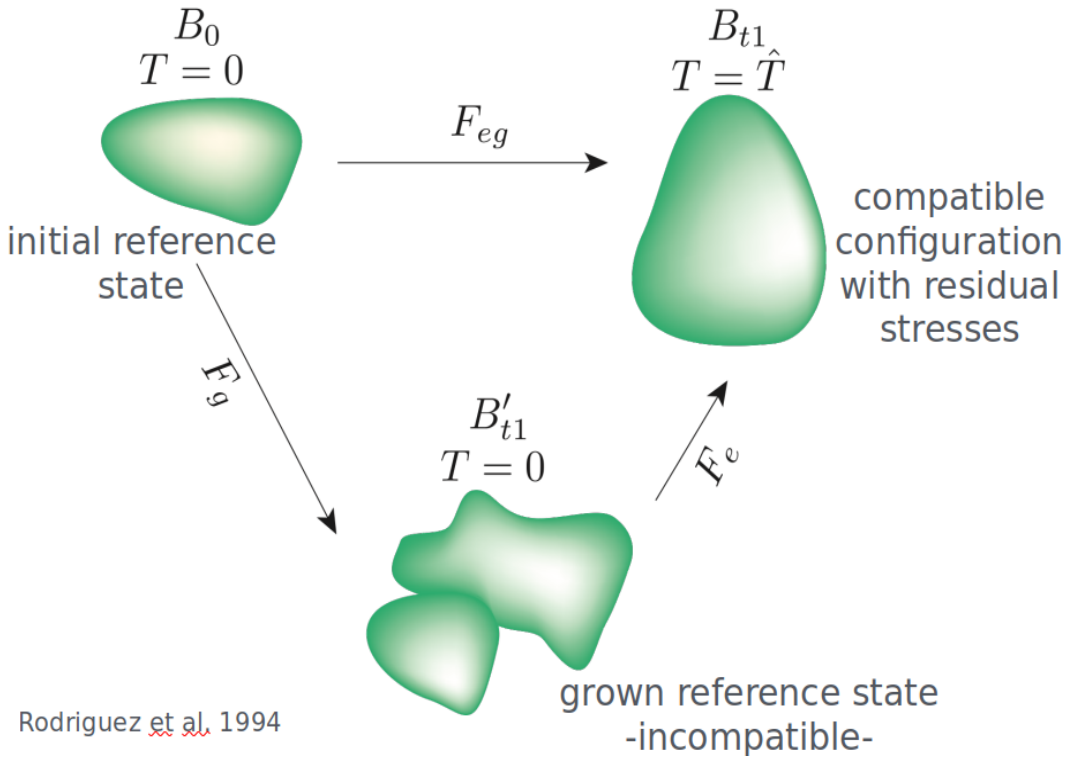

Figure 3.1: Growth as a combination of deformation and elasticity. The initial state B_o grows to a state B'_{t1} which has discontinuous and therefore incompatible to actually be observed. The observed state is B_{t1} is continuous and compatible with residual stresses present due to the elastic deformation (image courtesy Gabriella Mosca, shown with permission)

Thus we see that : Resultant growth is obtained as a combination of the Specified growth which would happen if a element developed independently from other elements and the elastic deformation which comes from the mechanical constraints. In essence, the elastic deformation acts as a constraint on the growth deformation, ensuring that it is compatible with the overall deformation of the system. In this approach, the hypothesis is that growth occurs in a quasi-static condition of mechanical equilibrium, as the timescale of growth is much larger.

3.1 MorphoMechanX

With MorphoMechanX, an AddOn for MorphoDynamX, biological tissues may be mechanically modeled using the Finite Element Method (FEM) for solid mechanics. MorphoMechanX, which is designed for components that grow and divide, differs from engineering FEM software in that it

allows growth and mechanics to interact with integrated genetic network simulations. The Thrust library, which uses Cuda on NVIDIA GPUs, allows for extreme parallelization of the applications. Gabriella Mosca's Doctoral research [21] has evolved into MorphoMechanX, which is sequentially being developed.

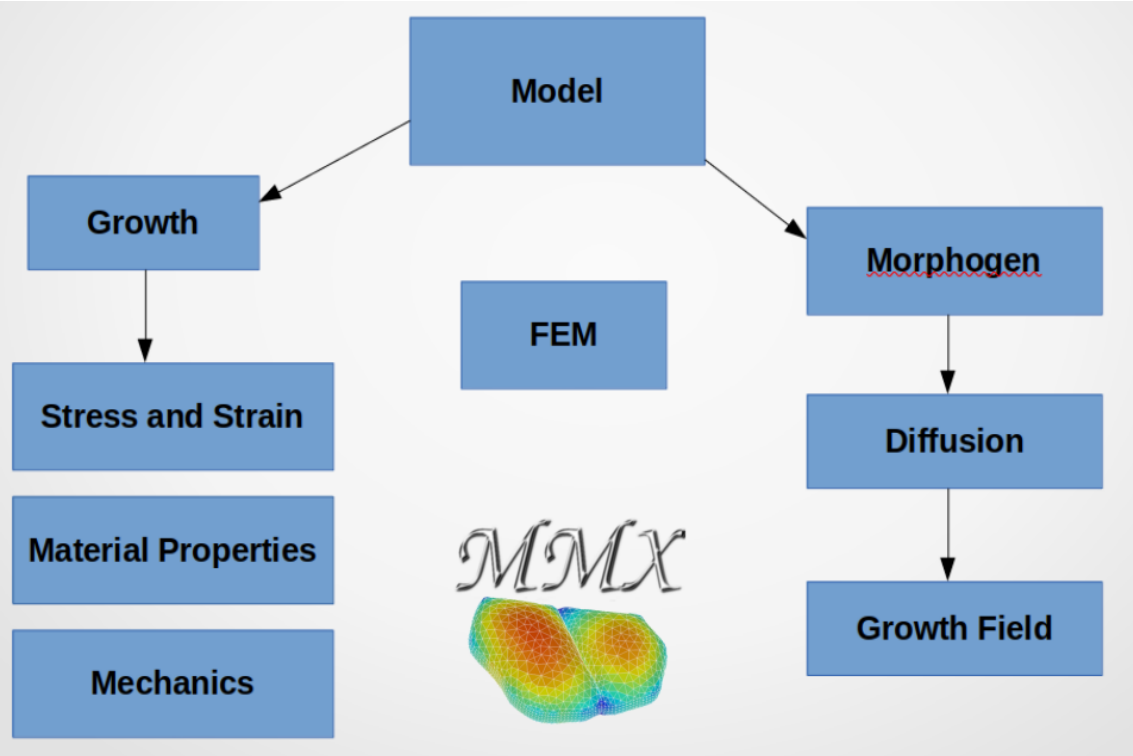

Figure 3.2: A simple flowchart of the modelling framework in this study

3.1.1 Mesh

Meshes are discretized representations of physical domains such as solid objects and fluid regions. The domain is divided into a number of smaller sub-domains known as elements, which are utilized to approximate the solution to a mathematical model of the physical system under investigation. A mesh is made up of nodes, which are points in space, and elements, which serve as the mesh's building pieces. The domain's geometry is defined by the nodes, and the elements link the nodes to form a finite element mesh. The element type, such as triangles or quadrilaterals in 2D or tetrahedra or hexahedra in 3D, is determined by the domain geometry and the analytic needs.

The mesh is a crucial part of the FEA process since it directly influences the analysis's accuracy and efficiency. A finer mesh with more nodes and pieces can yield a more accurate result, but it also raises the analysis's computing cost. A coarser mesh with fewer nodes and components, on the other hand, might lower computing cost but result in a less accurate solution. Meshing or discretization refers to the process of creating a mesh. The meshing technique and parameters, such as element size and mesh density, are chosen based on the geometry of the domain, the physics of the issue, and the analytic needs.

3.1.2 Cell Complex

Cell complexes are used to represent the geometry of the item being represented and to define how the geometric pieces are connected. Each member in the complex is given material qualities and is linked to its neighbors via common vertices or edges. The object's behavior is then approximated by solving a series of equations describing the forces and deformations of the various parts.

In FEM modeling, the use of cell complexes enables for the precise and efficient simulation of complicated mesh shapes and material characteristics. The model may be made more precise and capable of capturing complicated aspects of the item being represented by refining the cell complex through cell subdivision.

Mathematical cells of variable sizes make up the cell complex, which enables physical quantities with various intrinsic dimensions to be placed in the right places inside the framework. Local topological activities, such as the crucial procedure of cell division, may be performed on a cell complex and can be represented in an index-free manner. Additionally, the cell complex is built using neighborhood interactions, allowing developmental rules to conveniently access values in adjacent cells.

In order to provide a C++ API [22] that can be used to computationally describe development in any number of dimensions, the Cell Complex Framework makes use of this representation. Iterating through a cell complex, adding, deleting, splitting, and merging cells are only a few of the basic functions offered by the framework.

3.1.3 Processes

The majority of MorphoMechanX actions, including numerous menu items like saving a mesh, are executed by processes. They are located on the ”Process” tab [23], where they are organized in a hierarchical folder view: first in sub-tabs for stack, mesh, and Model processes, and then in folders below. When we pick a process, its accessible parameters are displayed in the box below. The project (.mdxv) file can be saved with changed parameter values.

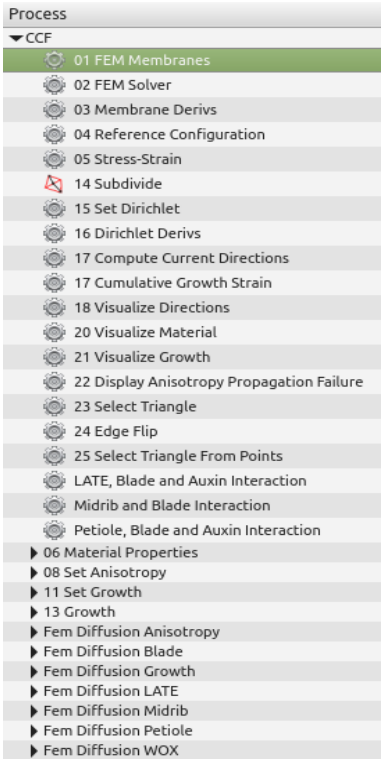

Figure 3.3: The Model Processes in the software are in a modular form which results in easy addition or removal without interference

3.2 Model

We now describe the set-up of the initial model mesh which is to be used with the model. The primary purpose of the model is to grow a leaf shape from a primordium. This later can be extended to other templates and desirable final results.

3.2.1 Reference Configuration

The process Model/CCF/04 Reference Configuration must be run with all of the mesh's faces selected in order to generate the mechanical elements for the FEM solver. In addition to creating the components, this operation also changes their reference configuration to reflect the present configuration. Although a thickness value has been assigned, it has been set to 1 mm because it has little significance in this 2D membrane simulation. This is because the membrane thickness will result in a global rescaling factor for the resulting forces rather than affecting the equilibrium configuration or stresses.

Resetting the reference configuration

Residual stress is a sort of stress that stays within a material or component even after external stressors are eliminated. Residual stress can have a detrimental impact on the performance of a material or component, hence it is typically desired to release or minimize it. Resetting the reference configuration is a way for releasing residual stress. The reference configuration for each growth phase is not the initial configuration, but rather the configuration gained in the preceding growth stage.

3.2.2 Material Properties

A model that connects stress and strain in a linear elastic material is the Saint Venant material law. It is also known as the linear material model and is a subset of the more generic hyperelastic material models. The stress in the linear elastic model is linearly proportional to the strain, and the proportionality constant is derived as the elastic modulus. The stress-strain relationship for an isotropic material may be stated as:

$$\sigma = E\varepsilon \tag{3.1}$$

where ε is the strain, σ is the stress and E is the elastic modulus. σ and ε are second-order tensors that represent stress and strain, respectively, in this equation.

In contrast, hyperelastic material models describe materials with non-linear stress-strain behavior. These models are used to explain materials that flex a lot, like rubber and other elastomers.

The Saint Venant material law can be changed to account for hyperelasticity by introducing new material characteristics that represent the material's nonlinear behavior. They describe Hooke's law in 3D in homogeneous and isotropic materials,

$$\sigma = 2\mu\varepsilon + \lambda \ \mathrm{tr}(\varepsilon)I, \tag{3.2}$$

where ε is the strain tensor, σ is the stress tensor and tr is the trace function. In terms of tensor components, Hooke's law may be expressed using index notation, as shown below.

$$\sigma_{ij} = 2\mu\varepsilon_{ij} + \lambda\delta_{ij}\varepsilon_{kk}, \tag{3.3}$$

I is the second order unit tensor and λ and μ are the Lamé constants.

For the Saint Venant–Kirchhoff model, the strain-energy density function is

$$\psi(E) = \frac{\lambda}{2}[\mathrm{tr}(E)]^2 + \mu\mathrm{tr}\left(E^2\right) - \mu ln(detE) \tag{3.4}$$

where E is the Lagrangian Green strain.

The first term in the strain energy density function indicates the contribution of the strain component, while the second term represents the contribution of the volumetric component of the strain. The third term is a penalty term that assures the deformation is isochoric (volume-preserving).

The stress-strain relationship for the hyperelastic material may be determined by considering the derivatives of the strain energy density function with respect to the strain components. This relationship is nonlinear and is affected by the material's deformation state.

First, the intensity of the Young modulus in the fiber direction (E2) and the isotropic plane (designated E1E3 in the model) must be assigned. The Model/CCF/06a Material Properties Uniform procedure determines global Young modulus and Poisson ratio values. The specified template must be executed with the fields [1] 'Young E1E3' set to '100,' 'E2' set to '100,' and 'Poisson' set to '0.3'.

3.2.3 Stress - Strain

The motion of a continuum body and its deformation were discussed in some detail in Chapter 2. These processes cause interactions between nearby materials inside the body, which in turn generate stress - a force per unit of area - which is essential in continuum mechanics to comprehend material deformation.
Here, we introduce the notion of stress and explicitly consider a deformable entity that experiences limited motion.
Stress is commonly determined using the finite element approach by post-processing the nodal values of the finite element solution. The stress at a certain location in the domain is computed by taking the gradient of the displacement field with respect to the material coordinates and multiplying it by the solid's material parameters. Differentiating the strain energy density function with regard to the strain components yields the connection between stress and strain in hyperelastic materials.

First Piola–Kirchhoff stress

The first Piola-Kirchhoff stress tensor can be obtained using the deformation gradient. If $\psi(F)$ is the strain energy density function, the 1st Piola–Kirchhoff stress tensor can be calculated for a hyperelastic material as

$$P = \frac{\partial \psi}{\partial F} \qquad \text{or} \qquad P_{iK} = \frac{\partial \psi}{\partial F_{iK}}. \tag{3.5}$$

where F is the deformation gradient.

Cauchy stress

The Cauchy stress is determined by

$$\sigma = \frac{1}{J}\,\frac{\partial \psi}{\partial F} \cdot F^{\mathsf{T}}\ ;\ \ J := \det F \qquad \text{or} \qquad \sigma_{ij} = \frac{1}{J}\,\frac{\partial \psi}{\partial F_{iK}}\,F_{jK}\ . \tag{3.6}$$

To create a continuous stress field, the stress components can be assessed at each node in the domain and then interpolated over each element. The precision of the stress calculation is determined by the accuracy of the displacement field produced from the finite element analysis, the element

type and mesh density utilized, and the material parameters used in the constitutive equations.

3.3 Diffusion

Diffusion is a physical phenomena that occurs when particles or molecules migrate from high concentration areas to low concentration areas due to random molecular motion. Diffusion is significant in many natural processes, including food and waste product movement in cells, gas diffusion in the environment, heat diffusion in materials, and morphogen diffusion in biological responses [24].

Morphogens are also important in leaf formation and growth [25]. The significance of the plant hormone auxin in leaf patterning is one of the most well-studied instances. Auxin is created in the shoot apical meristem (SAM) and is polarly transferred to the base of the leaf primordium [26]. This leads to the establishment of a concentration gradient of AUXIN which represents the auxin driven PD growth rate plus the slowing down of growth that originates from the leaf tip. This specific distribution can be achieved by a diffusive field. Specified growth is felicitated by morphogens which are spatially distributed according to the initial conditions over the initial primordium template.

The diffusion equation, a second-order partial differential equation that relates the rate of change of a substance's concentration or density to its spatial distribution and time, can describe the basic mechanism of diffusion. Fick's first and second laws of diffusion [27], which characterize the flow and rate of diffusion, are mathematically expressed in the diffusion equation. Several parameters characterize the diffusion process, including the diffusion coefficient, which measures the ease with which particles or molecules can move through the medium, the concentration gradient, which measures the difference in concentration between two points, and the distance traveled by the particles or molecules.

Fick's second law describes how diffusion effects concentration to alter over time. It is a partial differential equation in one dimension that goes like this:

$$\frac{\partial \varphi}{\partial t} = D \frac{\partial^2 \varphi}{\partial x^2} + a - b\varphi \tag{3.7}$$

where φ is the concentration; $\varphi = \varphi(x,t)$ is a function, D is the diffusion coefficient, x is the position, a is the production rate, and b is the decay rate. In two or more dimensions, we must use the Laplacian $\Delta = \nabla^2$, which generalizes the second derivative, resulting in the equation

$$\frac{\partial \varphi}{\partial t} = D\Delta\varphi \frac{\partial \varphi}{\partial t} = D\Delta\varphi + a - b\varphi \tag{3.8}$$

By discretizing the physical domain into small finite elements and numerically solving the diffusion equation on each, FEM may be used to describe and simulate diffusion processes on each element. A system of linear equations that connects the concentration or density at each node to the values at surrounding nodes is constructed using the finite element approach for diffusion. The density distribution or concentration of the material that is diffusing across time and space is determined by the system of equations' solution.

3.4 Finite Element Modelling

In engineering and science, partial differential equations (PDEs) are solved numerically using the finite element method (FEM). In disciplines including solid mechanics, fluid dynamics, and electromagnetics, it is a useful tool for modeling and evaluating complicated systems and structures.

A complicated system or structure can be divided into a finite number of simpler, linked components, known as elements, using the finite element approach. A collection of equations that link the nodal values of the solution variables (such displacement, velocity, temperature, or pressure) inside each element serve to characterize it. A bigger system of equations is then constructed from the individual equations to explain the behavior of the overall system.

The FEM involves several steps [28]:

- Discretization: A finite number of elements, each of which is specified by a collection of nodal points, are used to discretize the continuous domain.
- Approximation: A finite set of basis functions (often polynomials), whose coefficients are unknown, are used to approximate each element's solution.
- Formulation: The governing equations are applied to each element to generate the element

equations.

- Assembly: A bigger system of equations that explains the behavior of the complete system is created from the element equations.
- Solution: To determine the nodal values of the solution variables, the system of equations is solved.
- Post-processing: The solution is shown using contour plots, animations, or other visualization techniques utilizing the nodal values to compute additional variables of interest, such as stresses, strains, or fluxes.

The FEM is a flexible approach that can solve a variety of issues with challenging boundary conditions and geometries. Moreover, it may include a number of physical phenomena including contact, multiphysics coupling, or material nonlinearity. Yet, it necessitates a substantial investment in computing power, particularly for large-scale issues, and may entail a number of error causes, including mesh distortion, numerical instability, and modeling simplifications. In order to obtain more precise and trustworthy findings, the FEM is frequently used in conjunction with other techniques like experimental testing, analytical modeling, or optimization algorithms.

3.4.1 Weak Form

The FEM is based on a variational principle that seeks to find the solution that minimizes the energy functional associated with the PDE.

The mathematical formulation of the variational principle is weak form of the FEM, which allows for the use of piecewise continuous trial functions in the approximation of the solution. The weak form is derived by multiplying a test function to the governing PDE and integrating over the domain. This results in an integral equation that must be satisfied by the solution.

More specifically, let us consider the general form of a PDE:

$$L(u) = f \tag{3.9}$$

where L is a linear differential operator, u is the unknown function, and f is a known function. The weak form of the PDE can be derived by multiplying a test function v(x) on both sides of the

equation and integrating over the domain Ω:

$$\int_{\Omega} L(u)v(x)dx = \int_{\Omega} fv(x)dx \tag{3.10}$$

where dx is the integration measure over the domain Ω.

The test function v(x) is chosen as such that it satisfies certain boundary conditions and must be piecewise continuous over the domain Ω. The weak form allows for the use of such discontinuous functions in the approximation of the solution, which makes the FEM a powerful and versatile numerical method.

The weak form can be further simplified by using the Green's identity, which relates the integral of the product of the derivative of the function and the test function to the integral of the product of a function and its derivative. This leads to the following weak form for the PDE:

$$\int_{\Omega} \nabla u \cdot \nabla v dx - \int_{\Omega} fv dx = \int_{\partial\Omega} gv ds \tag{3.11}$$

where ∇ is the gradient operator, g is a known boundary condition, and ds is the surface measure over the boundary of the domain Ω.

The weak form can then be discretized using the finite element method, by approximating the solution u(x) and the test function v(x) using piecewise continuous functions over a finite element mesh.

3.4.2 Discretization

The partial differential equation (PDE) domain is partitioned into a finite number of subdomains, or "elements," for convenience. Typically, these components are straightforward geometrical structures like triangles or quadrilaterals in two dimensions, or tetrahedra or hexahedra in three dimensions. Meshing refers to the division of the domain into components 3.1.1.

When the integral form has been determined, the weak form is discretized. The integration is converted into a sum as the integral form must be solved numerically. The primary goal of discretization is to transform the integral form into a system of matrix equations that can be solved

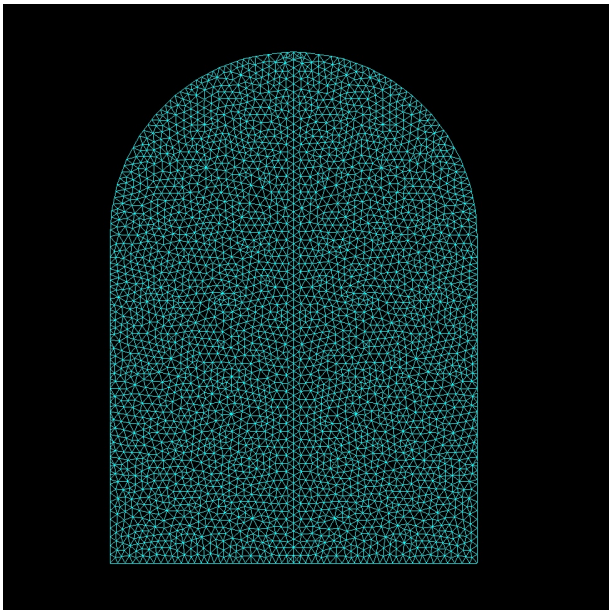

Figure 3.4: Discretized Mesh in the Model, shaped similar to the primordia

using well-known techniques of matrix algebra.

The next phase in the FEM is to estimate the PDE solution over each element using a set of basis functions once the mesh has been constructed. The basis functions are often continuous over each element and are typically polynomials of a specific degree, such as linear, quadratic, or cubic polynomials. The PDE's characteristics and the geometry of the issue influence the choice of basis functions. The nodal values of the solution at a finite number of discrete points, known as nodes, that are situated at the vertices of each element are used to determine the approximation of the solution over each element. The element-wise solution is built utilizing the basis functions and the nodal values of the solution.

This allows us to reduce the unknown functional u(x) to

$$u(x) = \sum_{i=1}^{n} N_i u_i \tag{3.12}$$

where n is the number of nodes in the element, u_i is the unknowns related to node i and N_i is the interpolation function.

3.4.3 2D Poisson

The Poisson equation in 2D can be written as:

$$\nabla^2 u(x,y) = f(x,y) \tag{3.13}$$

where u(x,y) is the unknown scalar field, f(x,y) is a given source term, and ∇^2 is the Laplace operator.

To solve this equation using FEM, we first discretize the domain Ω of the problem into a set of non-overlapping triangular or quadrilateral elements. Let Ω_e denote the element e, and let N_e be the set of nodes associated with Ω_e.

Next, we define a basis function $\phi_i(x,y)$ for each node i in N_e. The basis functions are usually chosen to be piecewise linear or quadratic functions, depending on the desired order of accuracy. These basis functions are typically chosen to satisfy the following properties:

- $\phi_i(x_j,y_j) = \delta_{ij}$, where δ_{ij} is the Kronecker delta.
- $\phi_i(x,y)$ is continuous and piecewise smooth over the complete domain Ω.
- The gradient of $\phi_i(x,y)$ is continuous and piecewise smooth over Ω.

Using these basis functions, we can approximate the solution u(x,y) over Ω_e by a linear superposition of the basis functions:

$$u(x,y) = \bar{u}(x,y) = \sum_i u_i \phi_i(x,y) \tag{3.14}$$

where u_i are the nodal values of the solution.

To obtain the weak form of the Poisson equation, we multiply both sides of the equation by a test function v(x,y) and then integrate over the entire domain Ω:

$$\int_\Omega (\nabla^2 u) v d\Omega = \int_\Omega f v d\Omega \tag{3.15}$$

Using the divergence theorem, we can convert the Laplacian to a surface integral:

$$\int_\Omega (\nabla^2 u) v d\Omega = \int_{\partial\Omega} (\nabla u) \cdot n v dS - \int_\Omega (\nabla u) \cdot (\nabla v) d\Omega \tag{3.16}$$

where n represents the unit outward normal to the boundary of Ω.

Applying the finite element method, we approximate u and v over each element Ω_e by their nodal values and basis functions:

$$u(x,y) = \bar{u}(x,y) = \sum_i u_i \phi_i(x,y) \tag{3.17}$$

$$v(x,y) = \bar{v}(x,y) = \sum_j v_j \phi_j(x,y) \tag{3.18}$$

We substitute these approximations in the weak form of the equation and obtain the following element-level linear system:

$$K_e u_e = f_e \tag{3.19}$$

where u_e is the vector of nodal values for the solution over Ω_e, K_e is the element stiffness matrix and f_e is the element load vector. These matrices and vectors are computed as follows:

$$K_e(i,j) = \int_{\Omega_e} (\nabla \phi_i) \cdot (\nabla \phi_j) d\Omega \tag{3.20}$$

$$f_e(i) = \int_{\Omega_e} f \phi_i d\Omega \tag{3.21}$$

Once the element-level linear systems have been assembled for all elements, they can be combined to form the global linear system:

$$KU = F \tag{3.22}$$

where K is the global stiffness matrix and U is the vector of nodal values for the solution over the entire domain Ω, and F is the global load vector.

Many numerical techniques, including direct solvers and iterative solvers, may be used to solve the global linear system. Next, using numerical techniques like the conjugate gradient method, Jacobi method, or Gauss-Seidel method, this system of equations is solved repeatedly. By applying the basis functions to interpolate the solution across each element after the nodal values of the solution are known, we can calculate the error in the finite element approximation. Overall, FEM offers a strong approach for the 2D Poisson equation solution and is applicable to a wide range of physics, engineering, and other applications.

3.4.4 Dirichlet Conditions

In the context of solving the 2D Poisson equation, the Dirichlet boundary conditions are a set of equations that specify the value of the solution on the boundary of the domain. Specifically, the Dirichlet boundary conditions for the 2D Poisson equation can be shown as:

$$u(x,y) = g(x,y) \text{ on } \partial\Omega \tag{3.23}$$

where u(x,y) is the solution to the Poisson equation, g(x,y) is a given function that specifies the boundary values, and $\partial\Omega$ is the boundary of the domain Ω.

The Poisson equation is approximated using piecewise linear or higher-order basis functions once the domain is broken down into a collection of components. The finite element solution's boundary nodes, which are the nodes that reside on the domain's edge, are then subjected to constraints in order to impose the boundary conditions. Using the same basis functions that are used to approximation the solution in the domain's interior, the constraints are produced by interpolating the boundary values onto the border nodes. The Poisson equation's solution is greatly influenced by the Dirichlet boundary conditions. The Dirichlet boundary conditions enable the identification of the only Poisson equation solution that satisfies the given boundary values by defining the boundary values.

3.5 Growth

3.5.1 Growth Anisotropy

In computational models of tissue growth, it is often assumed that growth occurs anisotropically, meaning that the tissue grows more in certain directions than in others, as it is what is observed in nature. This anisotropy can arise from various sources, such as the anisotropic distribution of cells or fibers [29], or mechanical forces acting preferentially in certain directions [1].

In mathematical terms, anisotropic growth is typically modeled using a growth tensor, which is a second-order symmetric positive-definite matrix that encodes the direction and magnitude of growth at each point in the tissue. The growth tensor can be decomposed into its eigenvectors and

eigenvalues, which represent the directions and magnitudes of maximal growth, respectively.

Anisotropic growth can be incorporated into tissue growth models in various ways. One common approach is to use a strain-based growth law, where the growth tensor is related to the strain tensor, which describes the deformation of the tissue. This approach assumes that tissue growth is driven by mechanical forces, and that the tissue responds anisotropically to these forces.[30]

The growth tensor is typically updated at each step of the simulation based on the current state of the tissue, and is used to compute the new position and shape of the tissue. Anisotropic growth can lead to a wide range of morphological patterns, depending on the specific form of the growth law and the initial conditions of the tissue.

3.5.2 Growth Step

It is crucial to take into account every component of the deformation tensor in order to guarantee that the development process is appropriately shown in the model. The growth tensor's rotational components, in particular, need to be properly taken into account. Without sacrificing generality, it is assumed that the elasticity tensor absorbs all of the rotational components of the growth tensor. This makes sure that the only way to represent growth without a rotating component is through a stretch tensor.

We have:

1. signal based growth

2. strain based growth (which acts uniformly in this model), is a sort of relaxation of residual stresses

3. a total release of stress/strain by setting the current configuration to the reference

They can be all used in combination, but not necessarily, especially as total release of residual stresses is a special case.

Assuming F_E^n and F_G^n represent the elastic deformation tensor and growth deformation tensor respectively, and X_{n-1} is the reference configuration at the (n-1)th growth step, the global deformation F_{EG} at the nth growth step can be expressed as:

$$F_{EG}^n = F_E^n F_G^n X_{n-1} \tag{3.24}$$

The growth tensor F_G^n may generally be affected by the present body coordinates x_{n-1} or by the body's elastic deformation/stress, which is estimated from the prior reference configuration. In the simulations carried out in this study, growth consists of an isotropic strain-based component (K_{iso} Strain), an explicit anisotropic component that is specified by the user through two diffusive processes (one for the mediolateral growth intensity K_{per} and one for the proximodistal growth intensity K_{par}).

Connecting morphogen signal to growth attribute which acts on the lengths in the current configuration and is pulled back [17] to the original configuration

$$g_{kPar} += max((K_{Par} * (Signal) - kParSignalThresh, 0) \tag{3.25}$$

(We must note that scaling is cumulative. The scalings keep on adding as we apply the set growth process)

For this growth component, the growth tensor G_{KPar} is expressed in a diagonal basis:

$$G_{KPar} = \begin{bmatrix} 0 & 0 \\ 0 & g_{KPar} \end{bmatrix} \tag{3.26}$$

Here, g_{Kpar} stands for the local anisotropic growth coefficient in the direction parallel to Kpar.

A growth direction that is orthogonal to K_{Par} can be specified, however depending on the growth assumptions, this direction may not be orthogonal to K_{Par} in the present configuration even though it is in the reference configuration. An alternate method for dealing with this is to compute the diffusion process and its gradient at each development step in the current configuration and then transfer it onto the reference configuration.

The growth tensor G is a diagonal matrix with g_{KPar} and g_{KPer} as its diagonal elements.

$$G = \begin{bmatrix} g_{KPar} & 0 \\ 0 & g_{KPer} \end{bmatrix} \tag{3.27}$$

In the diagonal basis of G_{KPar}, the strain-based growth tensor G_E is represented. Thereafter, it is added to the simply anisotropic growth tensor (G) to create the global growth tensor G_{TOT}. The strain is calculated by mapping a vector from the reference configuration to a vector from the present configuration using the Green-Lagrange strain tensor [1].

A 2D rotation matrix is used to rotate the triangle represented in the current configuration in order to calculate G_E components. Then, eigenvalues and eigenvectors are determined from the Green-Lagrange strain tensor [18] between the reference triangle and the present triangle. Each in-plane eigenvalue is then subjected to an engineering strain calculation.

$$G_E^D = g_\varepsilon \begin{bmatrix} max(0, \varepsilon_{11}^E - \varepsilon_0^E) & 0 \\ 0 & max(0, \varepsilon_{22}^E - \varepsilon_0^E) \end{bmatrix} \tag{3.28}$$

$$\text{where} \quad \varepsilon_{ii}^E = -1 + \sqrt{(1 + 2\varepsilon_{ii})} \tag{3.29}$$

The diagonal representation of the strain-based growth matrix G_E^D is constructed using a growth proportionality factor g_ε and a threshold value ε_0^E below which there is no occurence of strain-based growth, where ε_{11}^E and ε_{22}^E are the ordered engineering strain eigenvalues derived from the ε_{11} and ε_{22} of the Green Lagrange strain.

Following that, the diagonalized G_{KPar} basis is used to represent the strain-based growth tensor,

$$G_E = R_{eigen}^T G_E^D R_{eigen} \tag{3.30}$$

where R_{eigen}^T is matrix with eigenvectors of Green-Lagrange strain as its columns and the resultant growth tensor G_{TOT} is calculated as

$$G_{TOT} = 1 + dt(G + G_E) \tag{3.31}$$

on the basis that diagonalizes G. Just the rest lengths are recorded since the triangle's spatial arrangement is unimportant and growing the triangle results from applying G_{TOT} to the reference triangle coordinates.

3.6 Mechanical Equilibrium

The system typically has to develop a new equilibrium configuration after each growth step that can accommodate both the pressure-induced stresses and the residual stresses produced by the growth process. By solving the governing partial differential equation (PDE) under the right boundary conditions, which guarantee that the structure is in a state of static equilibrium, the mechanical equilibrium is enforced in the FEM. This implies that the structure must balance the forces operating on it from the outside due to internal tensions.

To do this, a set of equilibrium equations that balance the internal stresses and external forces within each element must be used to link the nodal forces and displacements. By taking into account the forces operating on an element and the consequent stresses inside the element, these equilibrium equations are developed.

$$\Pi(U) = \Pi_{int}(U) + \Pi_{ext}(U) \tag{3.32}$$

$$\Pi_{int}(t) = \int_{\Omega_o} \psi(F(U))dV \tag{3.33}$$

$$\Pi_{ext} = -\int_{\partial\Omega_o} T \cdot U dS + \int_{\Omega_o} B \cdot U dV \tag{3.34}$$

We clearly state the reliance of F on u and write $F = F(u)$ from the equation Grad $U =$ Grad $x(X,t) -$ Grad $X = F(X,t) - I$. By the minimization of the strain energy with a semi-implicit Euler scheme [31], the equilibrium is calculated.

$$\nabla\Pi(U,\delta U) = D\Pi(u) = \frac{d}{d\varepsilon}\Pi(U + \varepsilon\delta U)|_{\varepsilon=0} = 0 \tag{3.35}$$

Chapter 4

Results

4.1 Simple Leaf Model

We attempted to created the simplest possible model which gives us comparable results to previous literature. [32, 16] provided inspiration for the model setup. As previously stated, the goal of this model was to start with a primordium template and simulate the growth of a young leaf which is 6-7 days old.

The three components of each model are:

- a canvas template with distributed factors based on a simple leaf primordium shape,
- a growth intensity polarity specification system, and
- a rule to perform growth (which is based to the specified growth and strain release, growth time step)

Three factors, AUXIN, BLADE, and a gradient of AUXIN, define the spatial domains of the initial canvas and supply the polarity information required to determine local growth orientations.

Along the middle of the leaf lamina, the growth rates in the proximodistal direction were examined from the obtained experimental data [16] in order to explain the observed growth patterns. From

proximal to distal locations, growth rates parallel to the midline first decline practically linearly. A two-dimensional model with a component named AUXIN was employed to explain these data. This factor regulates proximo-distal growth direction rescaled by a predetermined growth rate K_{par} and diminishes from proximal to distal places with an initial linear gradient. In the lateral domains, Higher areal growth rates are explained by the mediolateral factor BLADE, which encourages a growth rate K_{per}

$$X'_A = K_{par} X_A \tag{4.1}$$

$$X'_B = K_{per} X_B \tag{4.2}$$

Here X_A is the Auxin Signal and X_B is the Blade Signal

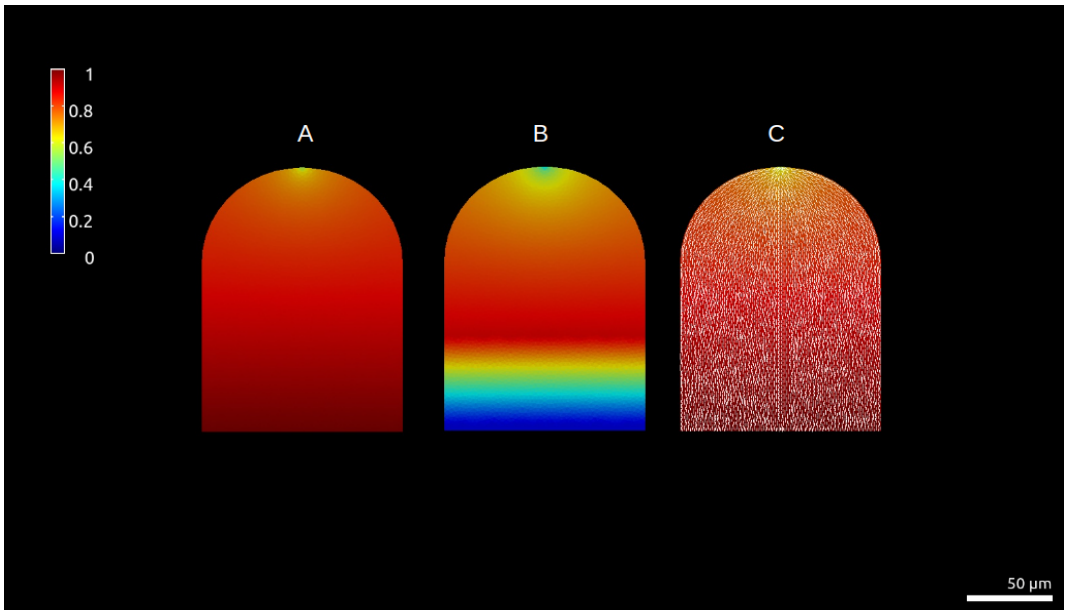

Figure 4.1: Morphogen Fields in Simple Model : A) AUXIN B) BLADE C) Growth Orientation (Scale Bar: 50 μm)

The two stated growth rates, parallel (K_{par}) and perpendicular (K_{per}) to the AUXIN gradient, are controlled by the user defined parameters. K_{per} is supported by BLADE whereas K_{par} is under the management of AUXIN. The mechanical connections between the tissue sections provide a canvas that makes it possible to calculate the deformation brought on by certain local growth patterns.

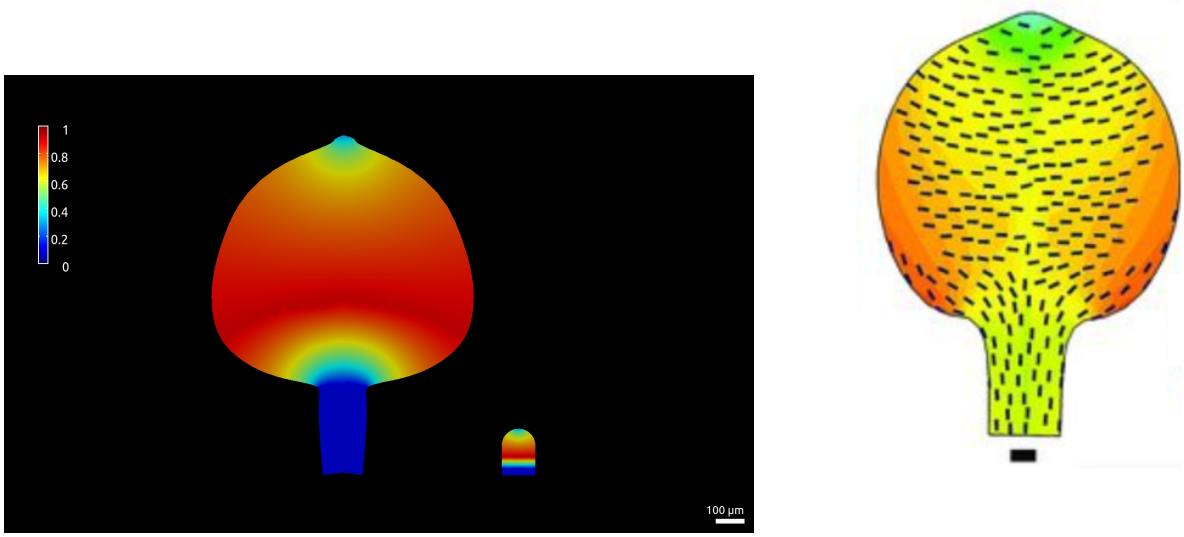

Figure 4.2: The grown leaf shape as the result of the model (visualised here the BLADE field), comparable to the previous model shape in [32] showing the resultant shape and growth rate. Note that our model does not have a midrib field yet which inhibits the growth rate in the middle portion (Scale Bar: 100 μm)

A parameter study of K_{par} and K_{per} was conducted to reach the desired leaf shape 4.3.

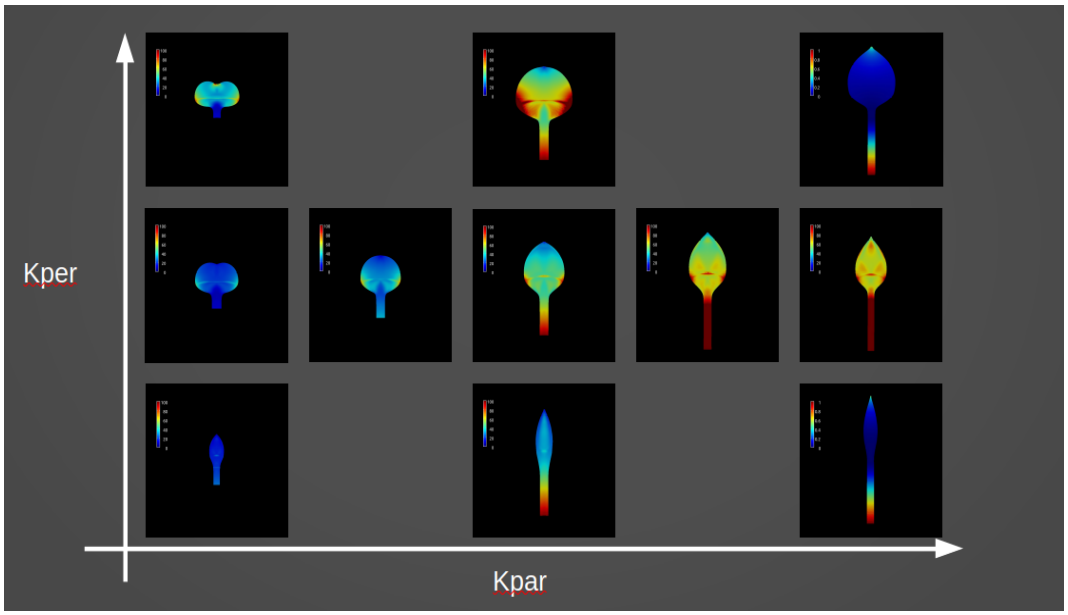

Figure 4.3: A parameter survey of the LeafGarden as the result of the model

The plant world is made of a myriad of distinct varieties in leaf forms. A plant species can be distinguished from other types of plants by the form of its leaves, which can also serve as an identifying trait. Using the simple model, it is possible to capture quite a number of different shapes (as long as the leaf complexity does not increase: serrations, leaflets) which can be documented to create a LeafGarden for future reference.

4.2 Mesh Refinement

In the previous model, as the growth iterations were performed and the size of the template became multi fold, the triangle elements of the mesh became long and skewed. This could result in an error in computation of the interpolation functions and subsequently the values of the quantities as the accuracy, can be lost with a coarse mesh, possibly leading to artifacts while the template grew for an extended period of time.

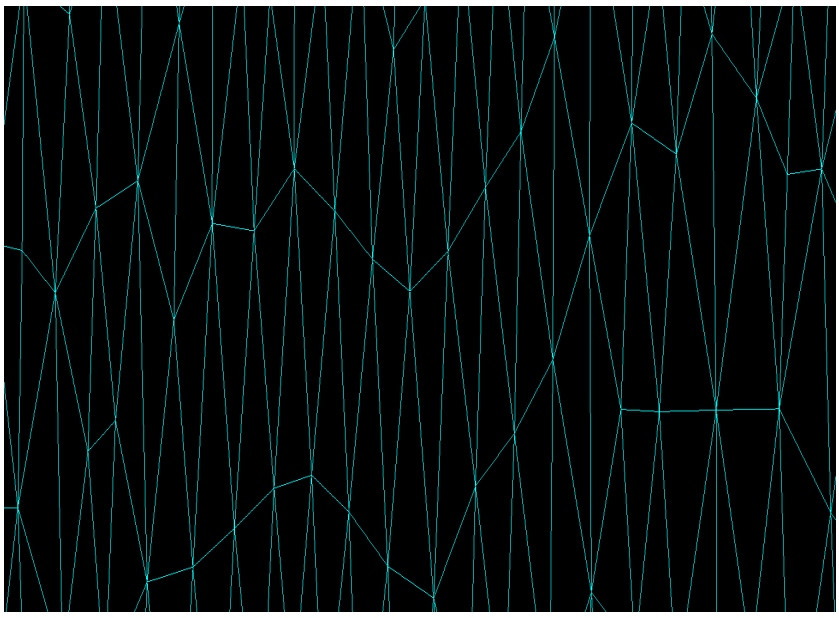

Figure 4.4: Triangle elements in mesh are error prone

Mesh refinement is the process of dividing the solution domain into smaller and smaller elements, with the goal of obtaining a more accurate approximation of the solution. Mesh refinement is necessary for these simulations for the following reasons:

- Accuracy: The accuracy of the answer increases as the mesh size lowers and the approximation error reduces. This is due to the piecewise polynomial approximation's ability to represent the behavior of the solution more effectively with lower element sizes.
- Numerical stability: In some cases, a coarse mesh can lead to numerical instability, which can cause the FEM solution to be inaccurate or even diverge. Mesh refinement can be used to improve the numerical stability of the FEM solution.

There are various mathematical techniques to do so, we discuss the ones we incorporated in the model. This was necessary as it could also be extrapolated to other models in this framework.

4.2.1 Subdivision

Mesh subdivision in finite element analysis refers to the process of refining a mesh by dividing the existing elements into smaller elements [33]. Mesh subdivision is used to increase the accuracy of the FEA solution, particularly in regions where the existing mesh is too coarse to accurately capture the physics of the problem.

There are several techniques for mesh subdivision, including:

- Uniform refinement: In this technique, each element is subdivided into a fixed number of smaller elements, resulting in a uniform increase in mesh density.
- Adaptive refinement: In this technique, the mesh is subdivided selectively based on local error estimates or other criteria.

Manual subdivision of meshes is possible. The mesh can be refined recursively by subdividing each element into smaller elements. The domain's geometry, the problem's physics, and the analysis' needs all influence the choice of subdivision technique and parameters, such as the maximum element size and level of refinement. A bisection algorithm is used to divide a triangle when its area in its present configuration exceeds a set limit (Max Triangle Size). This method divides the triangle's longest side into two equal pieces, and by joining the newly added vertex to the opposing one, it creates two new triangles. We must take into consideration conformity, which states that non-disjoint triangle intersections must have a shared vertex or side. By doing so, a conformal

mesh is ensured, and the subdivision can be propagated to neighboring triangles as described in [34].

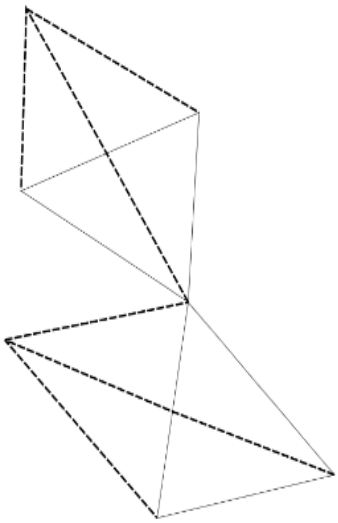

Figure 4.5: Conformality condition

One of the main benefits of a conformal mesh is that it accurately represents the physical system being modeled. This is because the mesh topology closely follows the geometry of the system, and the simulation can therefore capture fine features and details that may be missed by a non-conformal mesh. Another benefit of a conformal mesh is that it simplifies the modeling process. With a conformal mesh, the simulation domain can be easily divided into smaller elements that accurately capture the geometry. This makes it easier to simulate complex geometries and reduces the computational cost of the simulation. Furthermore, a conformal mesh ensures that there are no gaps or overlaps in the mesh, which can lead to numerical errors and inaccuracies.

Subdivision in the mesh create new triangle elements, edges and nodes. Such new geometrical entities are generated in the current configuration and only their position in this configuration. A triangle's edge, vertex, and other attributes must be propagated after each subdivision.

- In order for the Dirichlet requirement for mechanics and diffusion to apply to the newly inserted vertex, other vertex attributes must also do the same. The Dirichlet criteria set to the two vertices between which the new vertex is put will be passed on to the new vertex. Any Dirichlet conditions won't be inherited if that is the case.

- In the current configuration, an edge is divided into two equal parts, and each new edge inherits half of the undivided edge's length.
- As for material qualities, growth properties, anisotropy angles, and other characteristics, each smaller triangle inherits the same traits as the larger one.

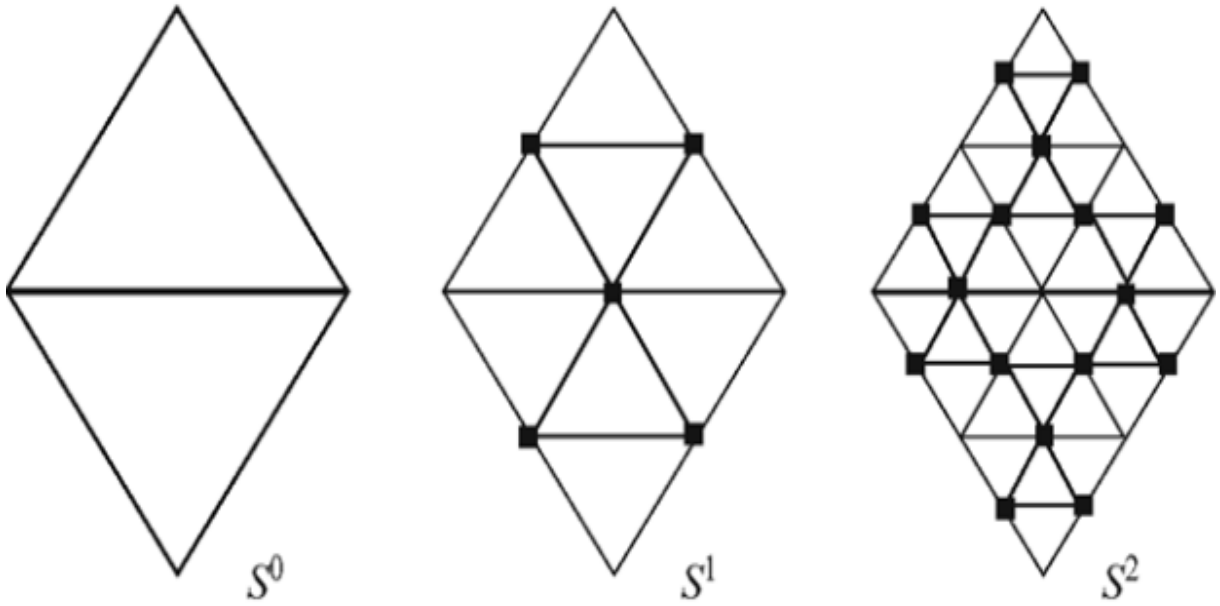

Figure 4.6: Levels of Subdivision, which lead to desired level of refinement

Overall, mesh subdivision is an important tool in FEA for improving the accuracy and reliability of the solution, particularly in regions where the existing mesh is too coarse. However, excessive subdivision can also lead to computational inefficiency and numerical instabilities, so it should be used judiciously.

4.2.2 Edge Flipping

Edge flipping is an operation that can be applied to a triangulation of a set of points to improve its quality. In a triangulation, an edge connects two vertices, and the edge flipping operation involves removing the edge and replacing it with another edge that connects two different vertices, thereby changing the triangulation [35]. Overall, the quality of the mesh is an important consideration in FEA because it affects the accuracy, reliability, and efficiency of the analysis. A well-designed and

well-constructed mesh is essential for obtaining meaningful results from FEA.

A collection of points in a plane can be triangulated using the geometric algorithm known as Delaunay triangulation. It creates a triangle so that none of the points in the set fall inside the angles of any of the triangles. The resulting triangulation is distinctive and maximizes the minimum angle of each triangle in the triangulation, making it a well-behaved mesh for many computational applications, including finite element analysis and computer graphics.

Several advantageous characteristics of the Delaunay triangulation include:

- In the Delaunay triangulation, no point lies inside the circumcircle of any triangle, which is known as the empty circumcircle property. For computational geometry algorithms, this property makes it especially useful.
- The triangles' circumcircles are as big as feasible, which implies that the Delaunay triangulation reduces the size of each triangle's largest circumcircle.
- The Delaunay triangulation is unique: given a collection of points, there is only one feasible Delaunay triangulation for those points. This is essential in mesh creation for computer simulations since it lowers the likelihood of singularities or other numerical instabilities.

Specifically, edge flipping is an operation that transforms a pair of triangles that share an edge into another pair of triangles by flipping the shared edge. In other words, given two adjacent triangles that share an edge, edge flipping removes the shared edge and replaces it with a different edge connecting the non-shared vertices of the two triangles, creating two new triangles.

Edge flipping can be used to improve the quality of a triangulation by improving the angles of the triangles. For example, if an edge in the triangulation creates a very acute angle between two triangles, flipping that edge can create two new triangles with more evenly distributed angles, which can lead to a more well-behaved mesh for various computational applications.

Edge flipping can be applied recursively to improve the quality of a triangulation until some stopping criterion is met, such as a desired minimum angle or a maximum number of iterations. However, edge flipping can also introduce new problems, such as creating non-Delaunay triangles, which violate the empty circumcircle property of the Delaunay triangulation [36]. Therefore, edge flipping should be used with caution and in conjunction with other quality improvement techniques.

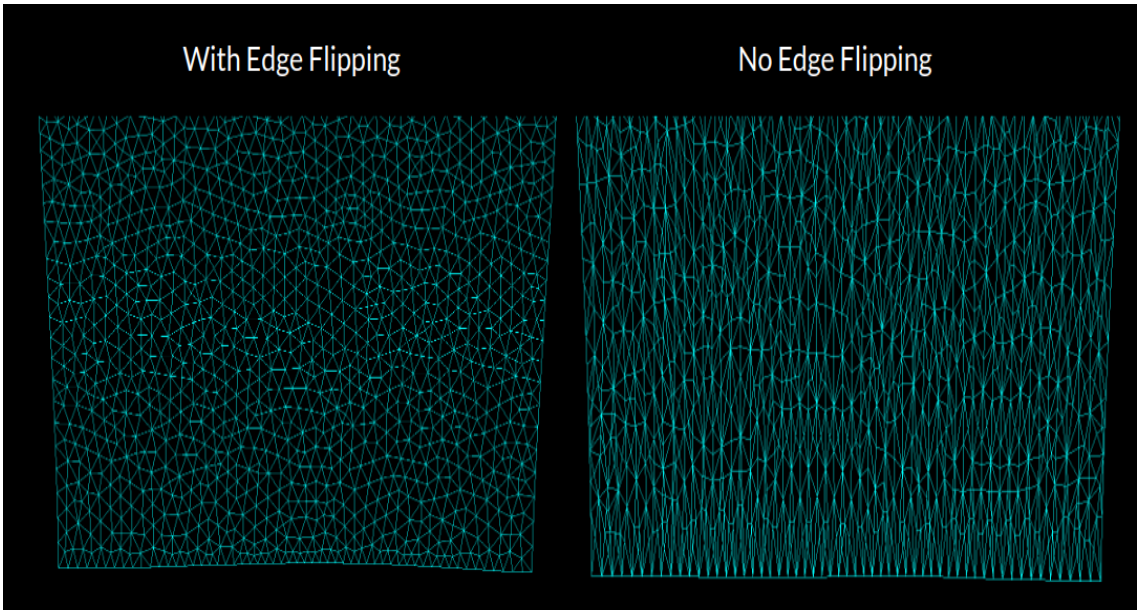

Figure 4.7: The effect of Edge Flipping to the mesh; it leads to more robust triangles (taken from the software)

Delaunay Criterion

The Circumcircle is a circle that is uniquely defined by a triangle formed from three non-collinear points. It completely encloses the associated triangle and has several noteworthy characteristics. For instance, a skinny triangle results in a larger circumcircle than a robust triangle of similar size. In skinny triangles, the area of the circle not covered by the triangle is proportionally larger than that in robust triangles. Additionally, the center of a circumcircle may extend beyond the associated triangle's region.

Circumcircles play a vital role in the Delaunay criterion's definition. [37] A Delaunay optimal triangulation requires non-degenerate triangles, which do not contain any other vertices in their circumcircle besides the three defining vertices.

If a vertex lies within a triangle's circumcircle, the triangulation may not be Delaunay optimal, and the network must be corrected. To restore optimality, a flip operation that switches the common edge between adjacent triangles is performed.

An important characteristic results from the aforementioned properties: If the total of the angles is less than or equal to 180 degrees ($\alpha + \gamma \leq 180°$), two triangles ABD and BCD with the common

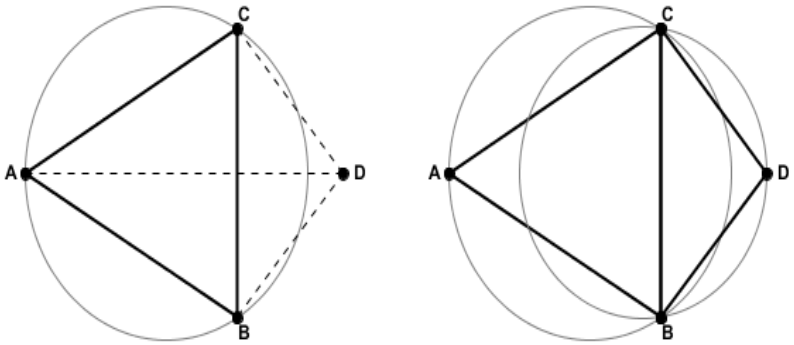

Figure 4.8: Delaunay Circumference Condition

edge BD satisfy the Delaunay condition.

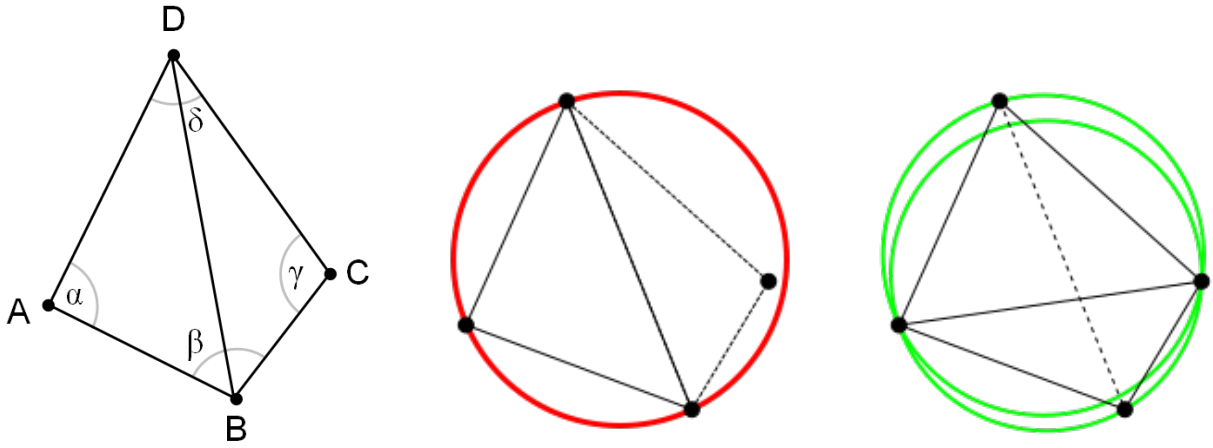

Figure 4.9: Figure A illustrates the Delaunay angle sum requirement for edge flip, Figure B illustrates a non-Delaunay triangulation in which the exterior vertex is within the circumference, and Figure C illustrates a Delaunay triangulation.

This is a crucial characteristic since it permits the application of the flipping approach. Switching the common edge BD for the common edge AC results in two triangles that do fulfill the Delaunay criterion if two triangles do not.

4.2.3 Smoothing

Mesh smoothing is a technique used in Finite Element Analysis to enhance the quality of a mesh. This technique is particularly helpful when the mesh is distorted or contains elements with irregular shapes or sizes that can result in inaccurate or unstable solutions. Mesh smoothing consists of modifying the positions of nodes in a mesh while maintaining the connectivity of the elements. The primary aim of mesh smoothing is to minimize element distortion and improve element quality by optimizing node positions.

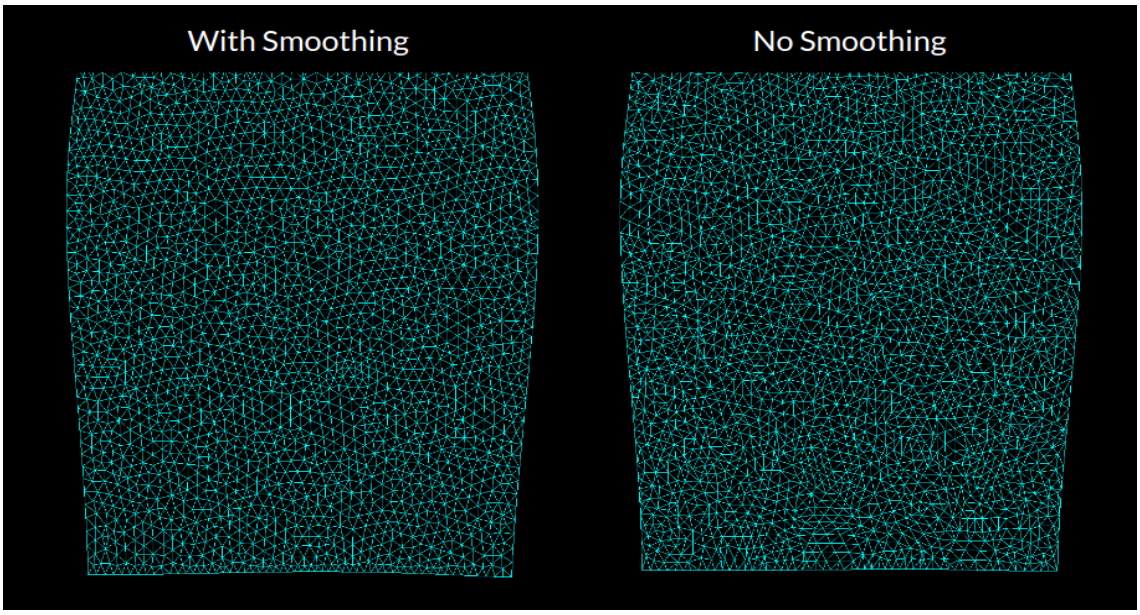

Figure 4.10: The effect of Smoothing to the mesh; it leads to better triangulations at the vertices (taken from the software)

Mesh smoothing can be done either manually or automatically using special software. The choice of smoothing technique and parameters depends on the geometry of the domain, the physics of the problem, and the analysis requirements. There are several methods for mesh smoothing, including Laplacian smoothing, optimization-based smoothing, and smoothing by subdivision. Laplacian smoothing adjusts the position of each node to the average position of its neighboring nodes, while optimization-based smoothing minimizes an objective function that measures element distortion or irregularity. In our model, we incorporate smoothing by subdivision which subdivides the mesh and then smooths it.

In conclusion, mesh smoothing is an important tool in FEA that helps to improve the quality and accuracy of a mesh. However, excessive smoothing can lead to loss of geometric detail, so it should be used with caution. When we do smoothing in our model, it is required in our software to release completely residual stresses and reset the reference configuration. This is something which would be nice to improve in the future, if a solution to the problem is found, which is possible for strictly 2D problems.

4.3 Kuchen LATE Model

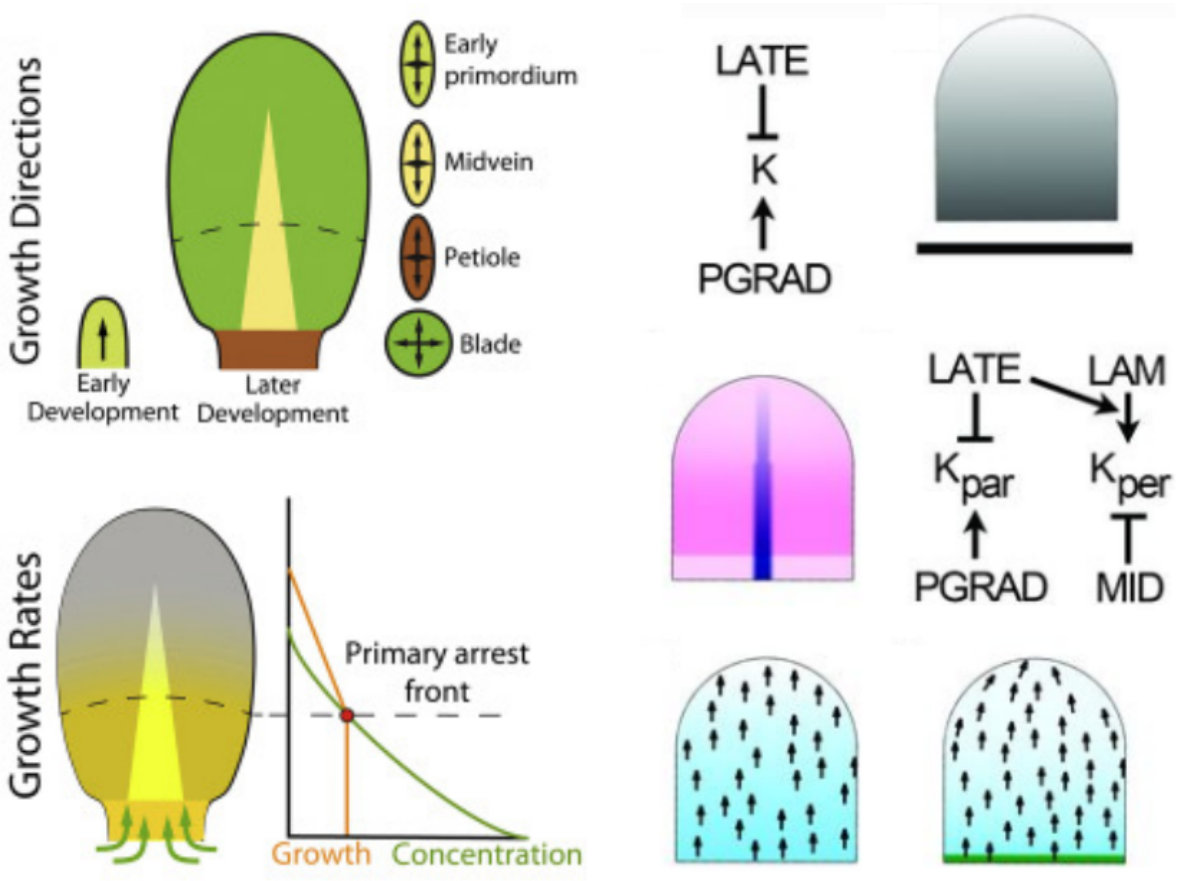

Figure 4.11: From Previous Modelling Approaches: Figure on the LEFT demonstrates the different growth rates desired in the primordia [16] and how they decrease as the growth occurs. Figure on the RIGHT demonstrates the growth intensity in the primordia and growth morphogen interaction scheme in [32] with different growth directions, if parallel is defined according to the y coordinate axis, or defined by the morphogen

Even though the generated leaves and gradients from the model 4.1 initially matched the data, the growth rates observed in later stages were not as high as predicted by the model. To address this issue, we incorporated additional factors into the model.

Specifically, we included MIDRIB, which is expressed in a triangular shape along the midline of the primordia and inhibits BLADE and subsequently Kper.

We also introduced a decaying field called LATE, which operates based on a threshold, that is the result of a diffusion problem with a self decaying term. This implies that while the domain is saturated, while the leaf grows, a region of lower LATE factor will appear. When the LATE values drop below the threshold during later stages due to the growth and deformation of the template, it inhibits the specified growth rates. LATE affects both AUXIN and BLADE (and so G_{par} and G_{per}). With these modifications, the resulting proximodistal growth rates better fit the data.

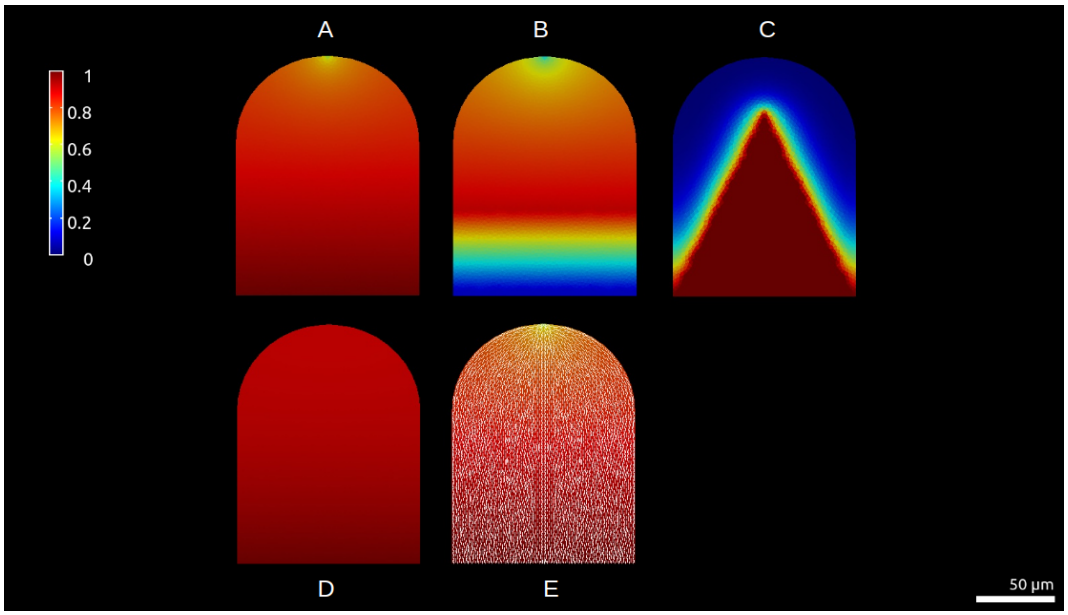

Figure 4.12: Initial Assigned Morphogen Fields in LATE Model : A) AUXIN B) BLADE C) MIDRIB D) LATE E) Growth Orientation (Scale Bar: 50 μm)

Midrib-Blade Interaction

As we see in section 3.5.2, the growth attribute for specified growth are translated from the morphogen signal concentrations after the diffusion process. Since we desire to have a Midrib field which inhibits the growth in mediolateral direction, we need to have a direct interaction between the respective morphogen fields

$$X_B = max\left(\frac{X_B}{1+\alpha X_M}, 0.1\right) \tag{4.3}$$

Here X_B is the Blade Signal, X_M is the Midrib Signal and α is a scaling factor.

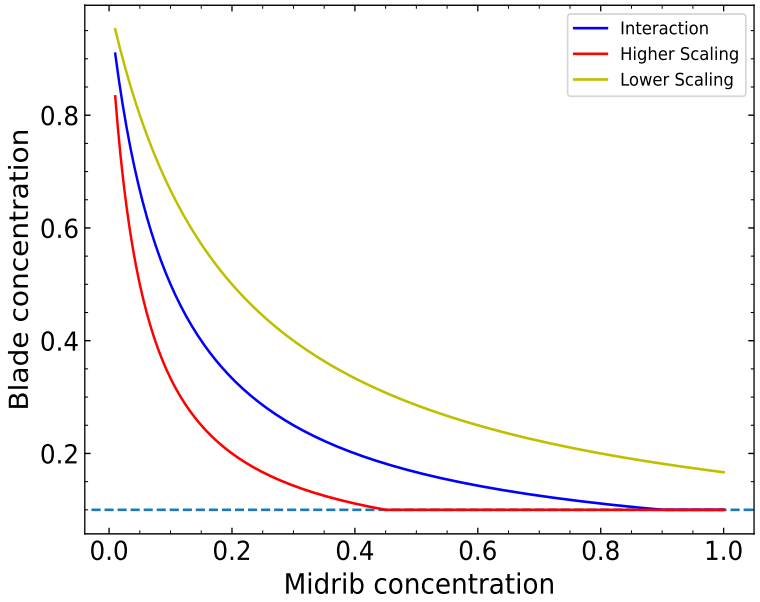

Figure 4.13: Midrib Blade Interaction with different scaling factors α

LATE-Auxin-Blade Interaction

Similarly for correctly using the functionality of the LATE field which reduces the growth rate in the leaf as the leaf grows, we have interactions between LATE and the respective morphogens

if($x_L < 1e-3$)

$$X_A = 0 \tag{4.4}$$

$$X_B = 0 \tag{4.5}$$

if $(1e-3 < x_L <= L_{th})$

$$X_A = X_A \frac{1+e^{\alpha}}{1+e^{\alpha * \frac{L_{th}}{X_L}}} \tag{4.6}$$

$$X_B = X_B \frac{1+e^{\beta}}{1+e^{\beta * \frac{L_{th}}{X_L}}} \tag{4.7}$$

if $(x_L > L_{th})$

$$X_A = X_A \tag{4.8}$$

$$X_B = X_B \tag{4.9}$$

Here X_A is the Auxin Signal, X_B is the Blade Signal, X_L is the LATE Signal and α and β are scaling factors for Auxin-LATE and Blade-LATE interactions respectively.

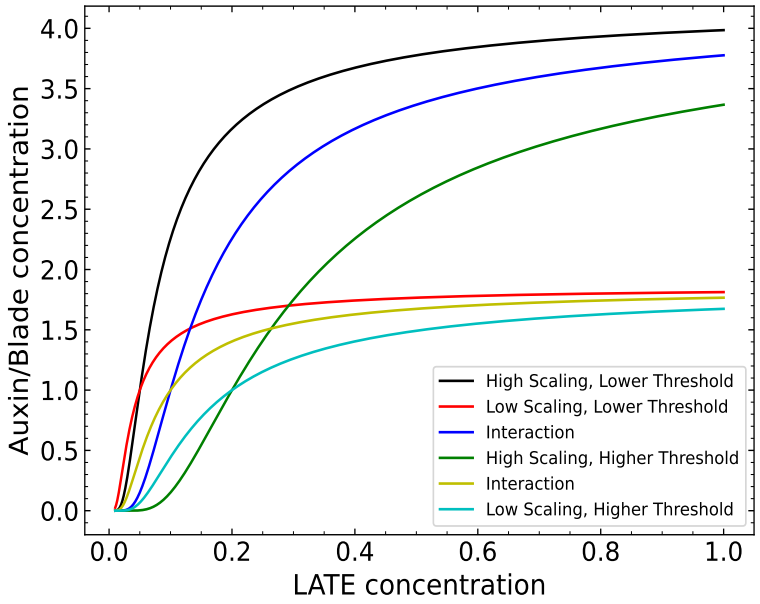

Figure 4.14: LATE-Auxin-Blade Interaction with different scaling factors α and β, and with different LATE Thresholds L_{th}

Having $K_{par} = 0.4$ and $K_{per} = 0.4$, with this model, we were able to grow LEAF1 of Arabidopsis Thaliana accurately.

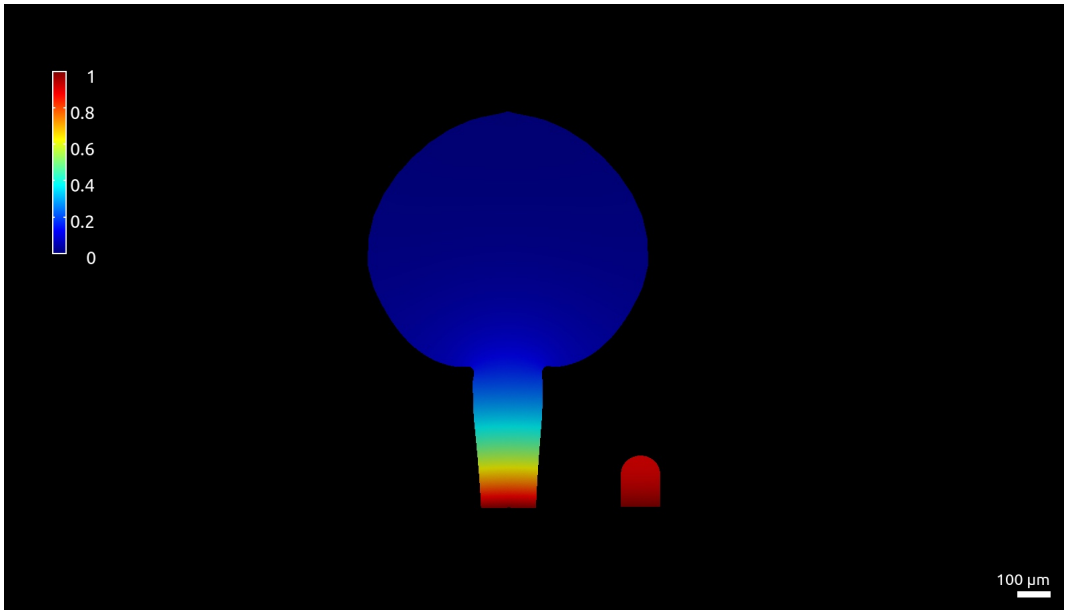

Figure 4.15: Grown LEAF1 in the LATE Model with the LATE field visualised compared to the initial primordia template size. As the template grows, the LATE field as a decaying quantity, becomes weaker (Scale Bar: 100 μm)

4.4 Petiole Model

To extend the validity of our model, we try to replicate the shape of LEAF8 of Arabidopsis Thaliana. As we saw in the introduction, Leaf heteroblasty becomes apparent during the transformation from embryonic leaves to true leaves. In Arabidopsis, the initial few true leaves are circular and small. With the plant's further development, the later leaves become elongated and more prominent, with evident serrations.

Leaf8 of Arabidopsis differs from the Leaf1 in the following measures

- Smaller size
- Smaller petiole
- Lower Growth Rates
- Visible marginal serrations

These are the features [38] which we wished to replicate accordingly. Serrations in the leaf would require an additional model for the margin cells [16], which our model currently doesn't have, thus we focus on the global shape (and not on smaller local features). We tried various methods to generate the shape from the LATE Model to account for the smaller petiole.

1. Flipping the Auxin Field

   This violates the growth rates observed in the biological data and also our initial assumption

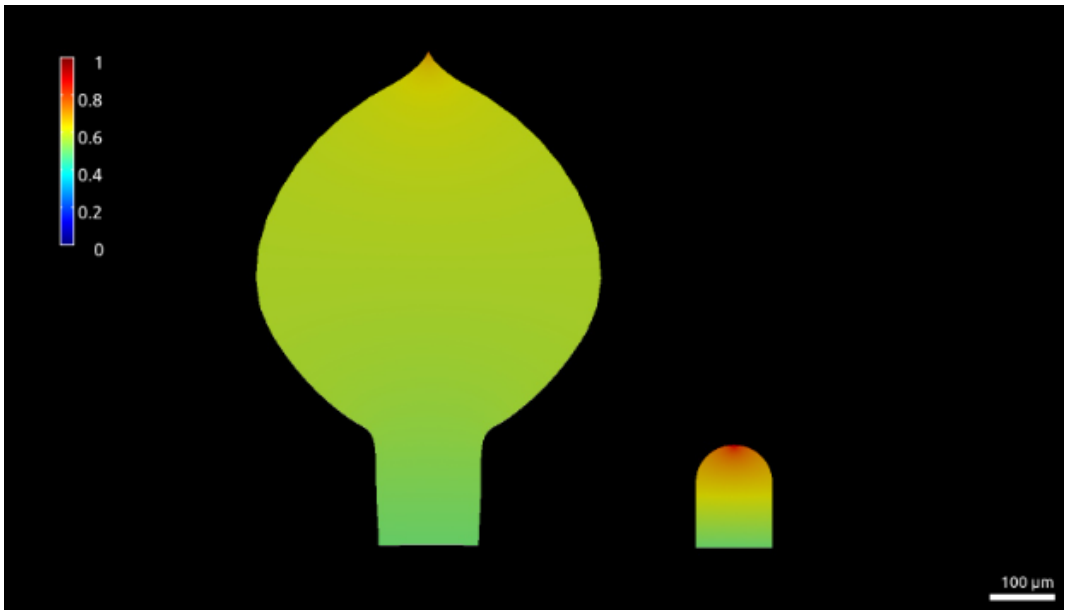

Figure 4.16: The reversed growth rates of the AUXIN field where the higher intensity is at the tip and lower intensity at the base

2. Flipping the function of the LATE Field

   The LATE field functions now in the case that growth at the initial stage is stunted and later the growth rates are increased, if LATE values are lower than threshold, growth rates are increased, resulting in the region where LATE values are higher to have lesser growth.

   This does not work; it violates the growth rates observed in the biological data

3. Reduce the Auxin Field Intensity

This reduces the overall leaf size, but the petiole to the blade proportion is still the same

4. Having Auxin Field similar to Blade

   This strategy results in weird outgrowths in the region where auxin maxima declines to lower values. Since the growth orientation follows the auxin field, it results in directional growth in that region of the primordia, leading to these outgrowths

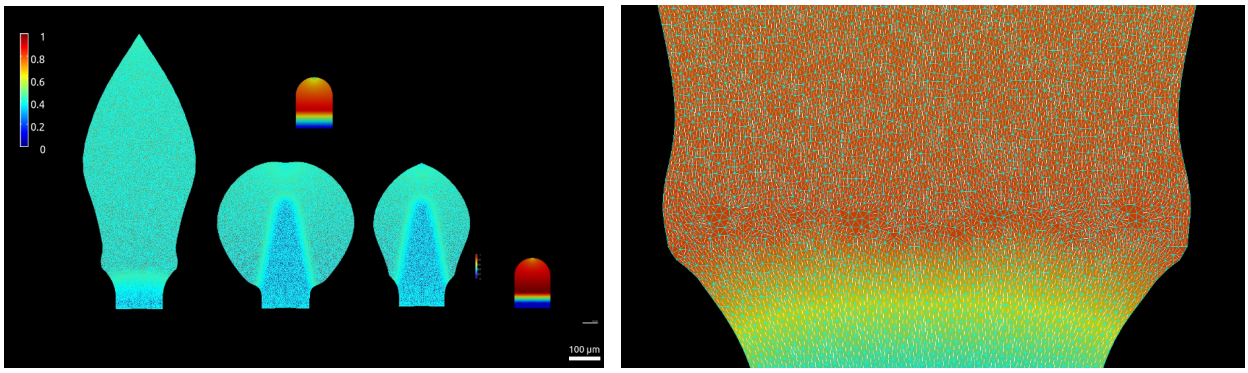

Figure 4.17: The Auxin field similar to the Blade leads to weird outgrowth at the blade-petiole boundary. This is due to the growth direction defined according to the AUXIN morphogen which leads to bad directions at the maximum-minimum boundary

We saw in Fig 4.11 that [32, 16] also had a dedicated petiole field. We had tried different model setups described above which could negate the need for a new field. However it was not possible to find a suitable configuration of fields and parameters which were biologically plausible. It seems clear that a new field is needed to counter the high growth of the petiole in LEAF1

As a benefit, this also helps in simplifying the BLADE field as it can now be defined similar to the AUXIN field as a proximodistal gradient

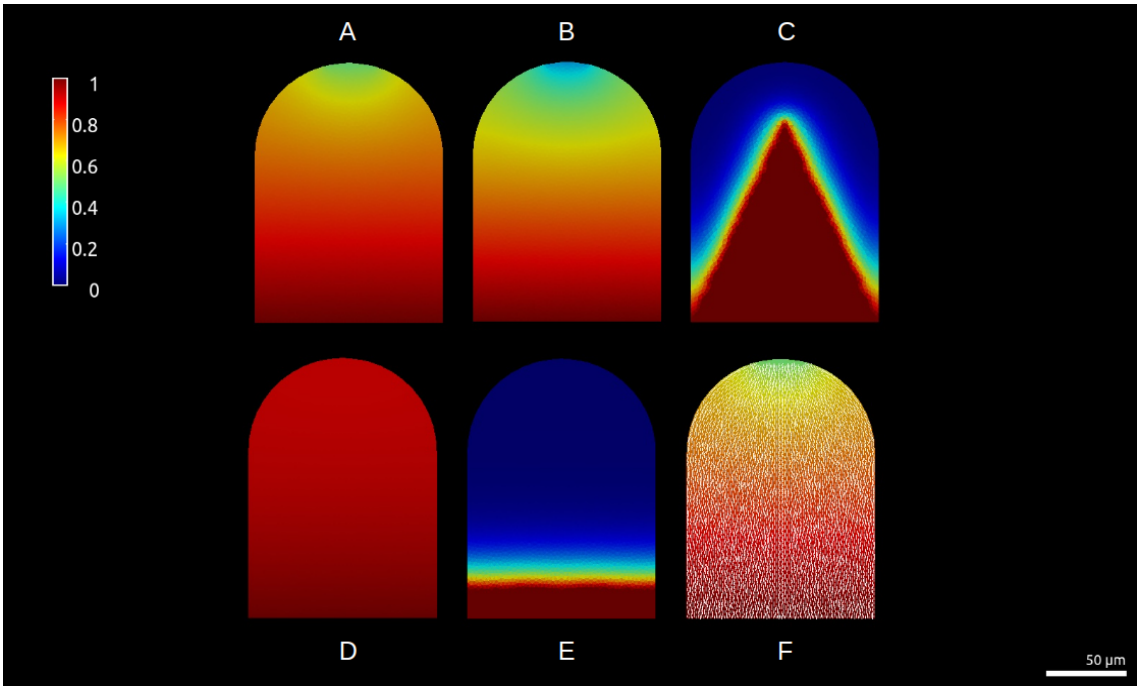

Figure 4.18: Initial Assigned Morphogen Fields in Petiole Model : A) AUXIN B) BLADE C) MIDRIB D) LATE E) PETIOLE F) Growth Orientation (Scale Bar: 50 μm)

Petiole-Auxin-Blade Interaction

$$X_A = \frac{X_A}{1+\alpha X_P} \tag{4.10}$$

$$X_B = max\left(\frac{X_B}{1+\alpha X_P}, 0.1\right) \tag{4.11}$$

Here X_A is the Auxin Signal, X_B is the Blade Signal, X_P is the Petiole Signal, and α and β are scaling factors for Auxin-Petiole and Blade-Petiole interactions respectively.

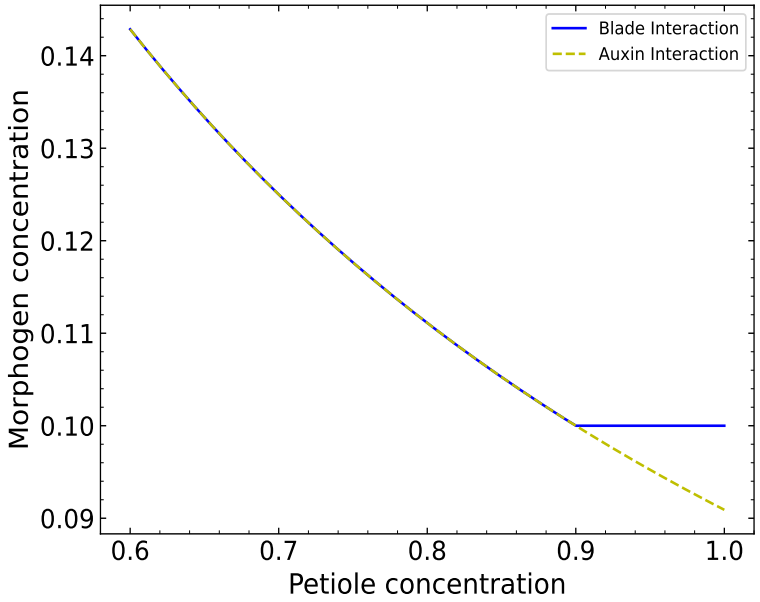

Figure 4.19: Petiole-Auxin-Blade Interaction which shows the different trends at the minimum concentration

With this model, we were able to grow LEAF8 of Arabidopsis Thaliana. This also helps in recreating the LEAF1 similar to the LATE Model. We use the real data to compare our leaf shapes. The proportions were replicated but the serrations on LEAF8 is an artifact only possible if we use a margin based differential growth scheme.

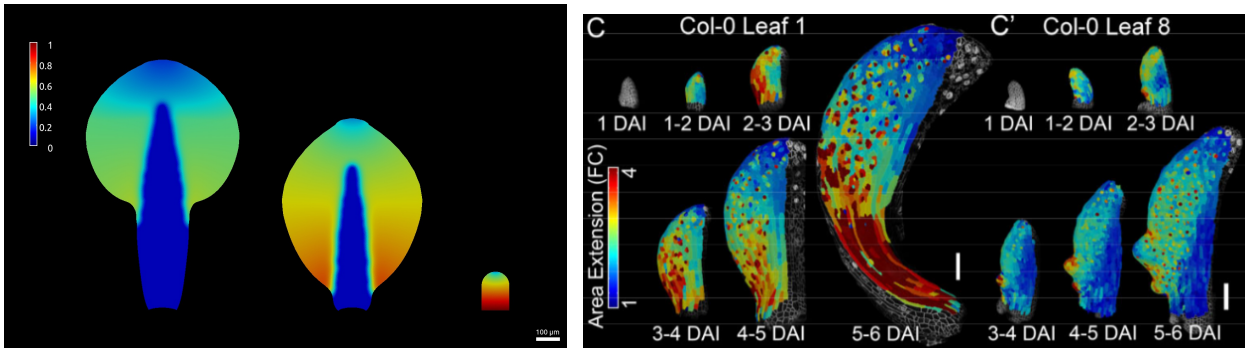

Figure 4.20: Figure A shows the LEAF1 and the LEAF8 created from the Petiole Model to compare with the real shapes (blade field visualised). Figure B demonstrates Experimental images of growth rates in LEAF1 and LEAF8 of Arabidopsis WildType at different time periods (image courtesy of MPIPZ, Scale Bar: 50 μm)

4.5 WOX Model

Recent research [39] provided a novel theoretical model for leaf production. The Wuschel-Related HomeoBox (WOX) gene controls the appearance of marginal cells and the development of leaf blades in Arabidopsis. In both monocots and eudicots, WOX genes are also in charge of regulating leaf width. Because of aberrant lateral growth, WOX mutants with their loss-of-function have a narrow leaf morphology. In Arabidopsis, WOX affect tissue identity to encourage lateral expansion, establishing a middle region that houses the leaf edge in the developing leaf primordia. However, it is unknown how growth control functions in relation to this domain delimitation mechanism and how WOX proteins govern certain facets of cellular development in the leaf. It is also unclear how WOX activity is distributed spatially and how the final form of the leaf result.

The proximally concentrated growth distribution and the lateral growth in the leaf blade that give A. thaliana leaves their distinctive ellipsoid form are controlled by the WOX genes.

We tested our model to be able to generate shapes in the proposed framework. The results are promising enough to continue to look in this direction.

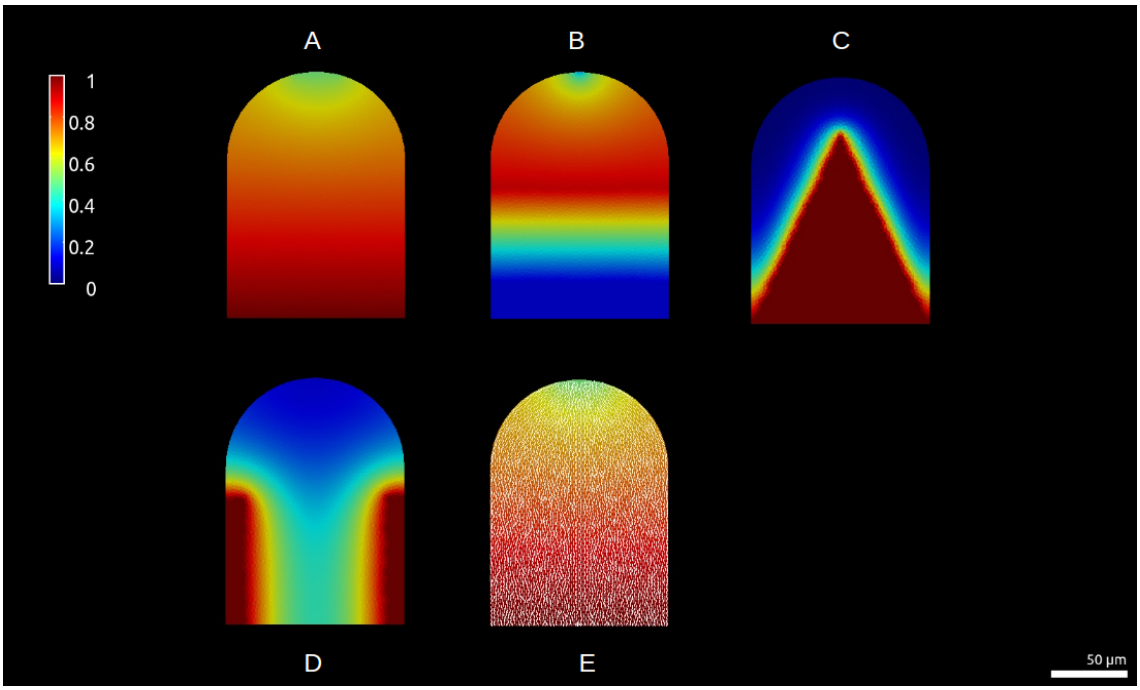

Figure 4.22: Initial Assigned Morphogen Fields in WOX Model : A) AUXIN B) BLADE C) MIDRIB D) WOX E) Growth Orientation (Scale Bar: 50 μm)

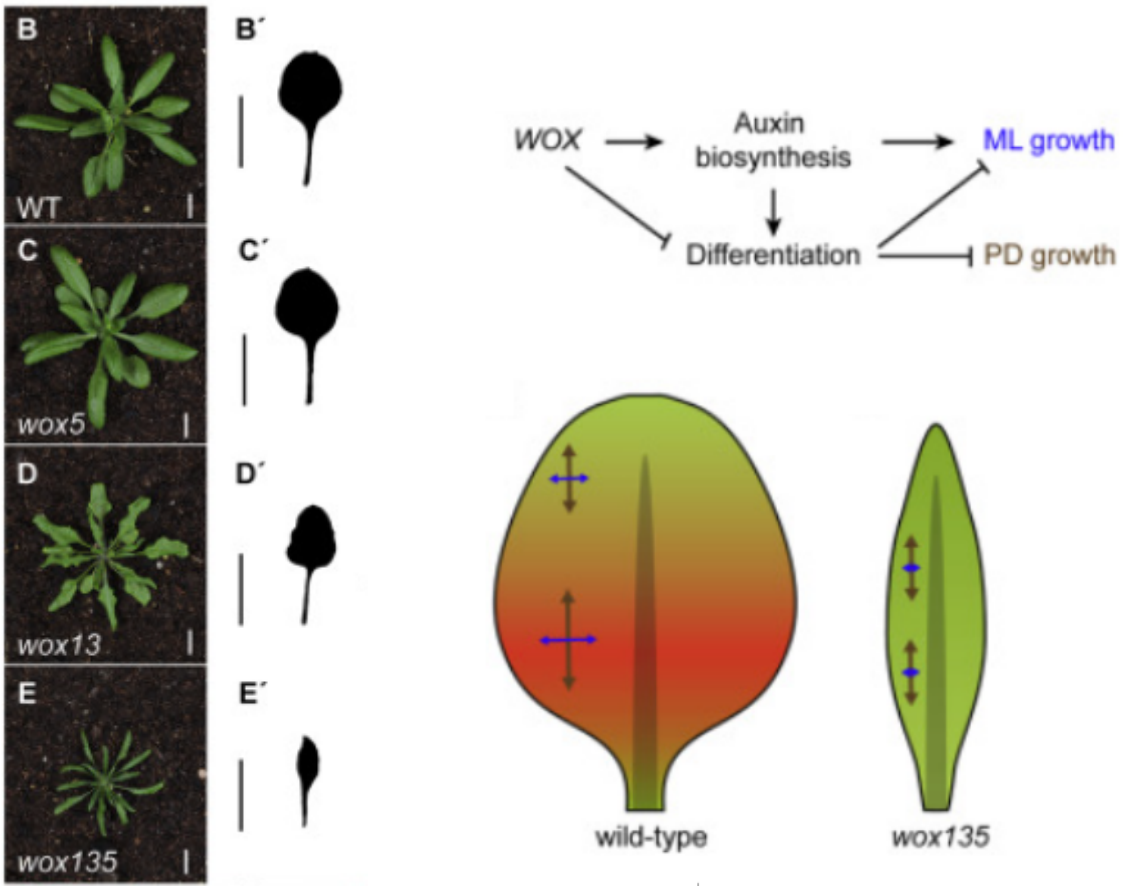

Figure 4.21: Figure A shows the effect of WOX genes to the leaf shape demonstrating the Wild-Type and the leaf blade of the WOX mutants with the absence of WOX genes. Figure B demonstrates Interpretation of wild-type and WOX mutant leaf shapes based on a conceptual model for the relationships between auxin biosynthesis, WOX, PD growth, ML growth, and segmentation during the formation of leaf blade (image adapted from [39])

WOX-Blade Interaction

$$X_B = X_B \times (1 + \alpha \times X_W) \tag{4.12}$$

Here X_B is the Blade Signal, X_W is the WOX Signal, and α is scaling factor for Blade-WOX interaction.

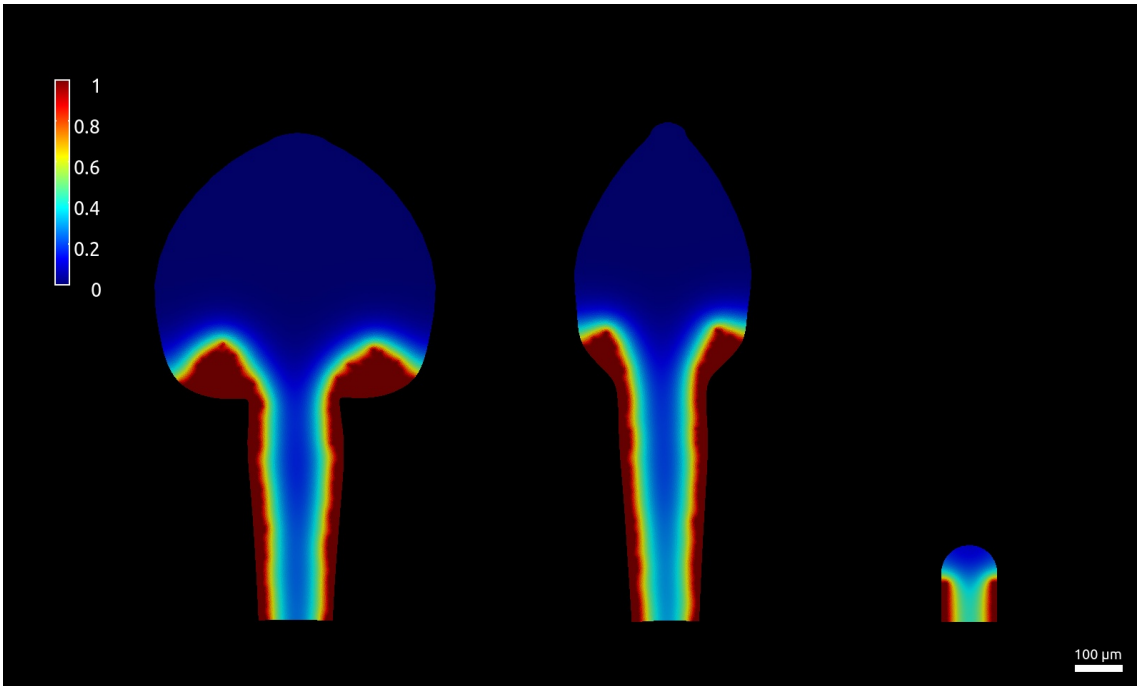

Figure 4.23: WOX Model final leaves shapes (Scale Bar: 100 μm)

Chapter 5

Conclusion

We thus created a functioning computational leaf model which replicates the results of various previous works. It was used to test out different theories based on real time data derived from experimental procedures. New Interactions and morphogen fields were created. Mesh refinement techniques were adapted for all models and fields. It was further developed for use by biologists and modellers alike to be able to simulate leaf growth for different purposes directly by changing the morphogen fields/growth rates inspired by the biological data.

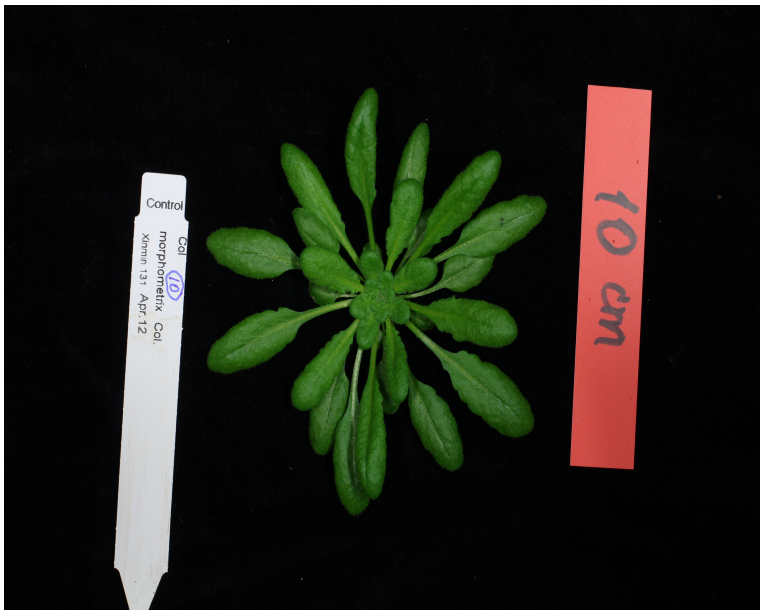

Figure 5.1: Leaf HeteroBlasty in Arabidopsis Thaliana (image courtesy XinMin Li, Scale Bar: 10 cm)

Modelling the structure and topology of leaves and other plant organs is a multidisciplinary field and an important component of biophysics:

Understanding leaf morphology: Leaf modeling can help us understand the variation in leaf shape, size, texture, and structure across different plant species. This information is important for plant identification and classification, and can also be used to study how plants have adapted to different environmental conditions. For example, plants in arid regions often have small, succulent leaves to minimize water loss, while plants in wetter environments may have large, broad leaves to capture more sunlight.

Photosynthesis: Leaves are the primary sites of photosynthesis in plants, where they absorb light and use it to convert carbon dioxide and water into glucose and oxygen. By studying leaf modeling, we can better understand the mechanisms behind photosynthesis, including the distribution of chloroplasts, the arrangement of veins, and the orientation of leaves. This knowledge can be applied to crop breeding and genetic engineering, to design plants that are more efficient at capturing sunlight and producing food.

Crop production: Leaf modeling can also help us improve crop production by understanding the relationship between leaf structure and function. For example, leaves that are more horizontal to the ground can capture more sunlight than those that are more vertical, while leaves with a greater surface area can absorb more carbon dioxide. By modeling leaf structure and function, we can optimize the design of crops for different growing conditions, such as in high-density planting or under low-light conditions.

Environmental monitoring: Leaf modeling can also be used to monitor the health of plants and the environment. Changes in leaf morphology can be an early indicator of environmental stress, such as drought, pollution, or nutrient deficiency. By monitoring the characteristics of leaves, we can detect these stressors early and take steps to mitigate their effects, such as by providing irrigation or fertilization.

Our initial problem of trying to compute the resultant growth as the outcome of specified growth is computationally resolved by this growth model. We can explain the final shapes and growth intensities from the results of the software and make attempts to understand a clearer picture of the connection. Replicating different leaves of different species on basis of the known GENE expres-

sions and the regulating network can be attempted and the learnings used to make the model more accurate.

The LeafGarden documented by multiple attempts of each model can serve as a future directory and template for other moodellers to build upon this work. The model also enables non-model-experts to try different paramters for the interactions to see its influence on leaf shape.

5.1 Future outlook

This model can be easily extended to include other angles such as cell-based modeling and growth where naturally shaped cells are modeled instead of cell complexes. A much interesting use of this work will be to test out theories of different growth schema and obtain the resultant growth as this software and the model provides us the tools.

Cumulative growth refers to the process of calculating and adding up growth rates over a certain period of time to determine the total growth or increase in a particular quantity or value. It is a useful measure for tracking the overall performance or progress of a system or entity over time as well as for forecasting future trends and projections.

Overall, cumulative growth is an important concept in biology where measuring and tracking changes over time is essential. It provides a simple and intuitive way to assess the total growth or increase in a quantity or value, taking into account the compounding effect of growth rates over time. A method for Growth Quantification was already in development at the time of writing and will be incorporated in the upcoming future.

Appendix

The models are saved in the gitlab folder (Model Thesis) and can be accesed with the above link. To run the models, it is required to have the MorphoDynamX package installed on the computer (MorphoMechanX).

Model Parameters

Parameters are saved in the .mdxv file in the respective model

1. LATE, Blade and Auxin Interaction 4.3

Parameter	Description	Value
LATE Signal	LATE Signal Name	LATE
Blade Signal	Blade Signal Name	Blade
Auxin Signal	Auxin Signal Name	Auxin
LATE Threshold	Threshold of LATE for Auxin and Blade Inhibition	0.05
Scaling Factor	Scaling Factor for Auxin and Blade Signal	2
Total time	number of iterations of the Model	800

Table 5.1: Parameter table for Process (saved in the .mdxv file)

2. Midrib and Blade Interaction 4.3

Parameter	Description	Value
Midrib Signal	Midrib Signal Name	Midrib
Blade Signal	Blade Signal Name	Blade
Auxin Signal	Auxin Signal Name	Auxin
Scaling Factor	Scaling Factor for Blade Signal	10.0

Table 5.2: Parameter table for Process (saved in the .mdxv file)

3. Petiole, Blade and Auxin Interaction 4.4

Parameter	Description	Value
Petiole Signal	Petiole Signal Name	Petiole
Blade Signal	Blade Signal Name	Blade
Auxin Signal	Auxin Signal Name	Auxin
Scaling Factor	Scaling Factor for Auxin Signal	10.0
Scaling Factor	Scaling Factor for Blade Signal	10.0

Table 5.3: Parameter table for Process (saved in the .mdxv file)

4. WOX, Blade and Auxin Interaction 4.5

Parameter	Description	Value
WOX Signal	WOX Signal Name	WOX
Blade Signal	Blade Signal Name	Blade
Auxin Signal	Auxin Signal Name	Auxin
Scaling Factor	Scaling Factor for Auxin Signal	0.2
Scaling Factor	Scaling Factor for Blade Signal	0.2

Table 5.4: Parameter table for Process (saved in the .mdxv file)

Bibliography

[1] Elvira Hernandez-Lagana, Gabriella Mosca, Ethel Mendocilla-Sato, Nuno Pires, Anja Frey, Alejandro Giraldo-Fonseca, Caroline Michaud, Ueli Grossniklaus, Olivier Hamant, Christophe Godin, Arezki Boudaoud, Daniel Grimanelli, Daphné Autran, and Célia Baroux. Organ geometry channels reproductive cell fate in the arabidopsis ovule primordium. *eLife*, 10:e66031, may 2021.

[2] Alan Mathison Turing. The chemical basis of morphogenesis. *Philosophical Transactions of the Royal Society of London. Series B, Biological Sciences*, 237(641):37–72, 1952.

[3] Michael J Crawley. *Plant ecology*. John Wiley & Sons, 2009.

[4] Neha Bhatia, Adam Runions, and Miltos Tsiantis. Leaf shape diversity: From genetic modules to computational models. *Annual Review of Plant Biology*, 72(1):325–356, 2021. PMID: 34143649.

[5] Gerhard Zotz, Kerstin Wilhelm, and Annette Becker. Heteroblasty—a review. *Botanical Review*, 77(2):109–151, 2011.

[6] Natalia Pabón-Mora and Favio González. Leaf development, metamorphic heteroblasty and heterophylly in berberis sl (berberidaceae). *The Botanical Review*, 78:463–489, 2012.

[7] Tsukaya H. Leaf shape: genetic controls and environmental factors. *The International journal of developmental biology*, 49(5):539–557, 03 2005.

[8] Bo Zhang and Donald L DeAngelis. An overview of agent-based models in plant biology and ecology. *Annals of Botany*, 126(4):539–557, 03 2020.

[9] Richard Kennaway, Enrico Coen, Amelia Green, and Andrew Bangham. Generation of diverse biological forms through combinatorial interactions between tissue polarity and growth. *PLOS Computational Biology*, 7(6):1–22, 06 2011.

[10] D Jeulin. Morphological modeling of images by sequential random functions. *Signal Processing*, 16(4):403–431, 1989. Special Issue on Advances in Mathematical Morphology.

[11] Paul Weiss and J. Lee Kavanau. A MODEL OF GROWTH AND GROWTH CONTROL IN MATHEMATICAL TERMS . *Journal of General Physiology*, 41(1):1–47, 09 1957.

[12] Siobhan A Braybrook and Cris Kuhlemeier. How a plant builds leaves. *The Plant Cell*, 22(4):1006–1018, 2010.

[13] Eran Sharon, Michael Marder, and Harry L Swinney. Leaves, flowers and garbage bags: Making waves. *American Scientist*, 92(3):254–261, 2004.

[14] Gemma D Bilsborough, Adam Runions, Michalis Barkoulas, Huw W Jenkins, Alice Hasson, Carla Galinha, Patrick Laufs, Angela Hay, Przemyslaw Prusinkiewicz, and Miltos Tsiantis. Model for the regulation of arabidopsis thaliana leaf margin development. *Proceedings of the National Academy of Sciences*, 108(8):3424–3429, 2011.

[15] Anne-Gaëlle Rolland-Lagan, Enrico Coen, Stephen J Impey, and J Andrew Bangham. A computational method for inferring growth parameters and shape changes during development based on clonal analysis. *Journal of Theoretical Biology*, 232(2):157–177, 2005.

[16] Daniel Kierzkowski, Adam Runions, Francesco Vuolo, Sören Strauss, Rena Lymbouridou, Anne-Lise Routier-Kierzkowska, David Wilson-Sánchez, Hannah Jenke, Carla Galinha, Gabriella Mosca, Zhongjuan Zhang, Claudia Canales, Raffaele Dello Ioio, Peter Huijser, Richard S. Smith, and Miltos Tsiantis. A growth-based framework for leaf shape development and diversity. *Cell*, 177(6):1405–1418.e17, 2019.

[17] Gerhard A. Holzapfel. Nonlinear solid mechanics: A continuum approach for engineering. pages 1–470, 04 2000.

[18] Larry Taber. Continuum Modeling in Mechanobiology . https://link.springer.com/content/pdf/10.1007/978-3-030-43209-6.pdf, 2020. [Online].

[19] Alain Goriely. The Mathematics and Mechanics of Biological Growth . https://link.springer.com/book/10.1007/978-0-387-87710-5, 2017. [Online].

[20] Eike Dohmen and Benjamin Kraus. Coupled anisotropic magneto-mechanical material model for structured magnetoactive materials. *Polymers*, 12(11), 2020.

[21] Gabriella Mosca. Modelling the mechanics of plant morphogenesis . http://gabriellamosca.altervista.org/joomla/aboutme/research, 2016. [Online].

[22] Brendan Lane. PhD Thesis; Cell Complexes: The Structure of Space and the Mathematics of Modularity . http://algorithmicbotany.org/papers/laneb.th2015.html, 2015. [Online].

[23] Pierre Barbier de Reuille, Anne-Lise Routier-Kierzkowska, Daniel Kierzkowski, George W Bassel, Thierry Schüpbach, Gerardo Tauriello, Namrata Bajpai, Sören Strauss, Alain Weber, Annamaria Kiss, Agata Burian, Hugo Hofhuis, Aleksandra Sapala, Marcin Lipowczan, Maria B Heimlicher, Sarah Robinson, Emmanuelle M Bayer, Konrad Basler, Petros Koumoutsakos, Adrienne HK Roeder, Tinri Aegerter-Wilmsen, Naomi Nakayama, Miltos Tsiantis, Angela Hay, Dorota Kwiatkowska, Ioannis Xenarios, Cris Kuhlemeier, and Richard S Smith. Morphographx: A platform for quantifying morphogenesis in 4d. *eLife*, 4:e05864, may 2015.

[24] Arnab Rai Choudhuri et al. *The physics of fluids and plasmas: an introduction for astrophysicists*. Cambridge University Press, 1998.

[25] Olivier Ali, Vincent Mirabet, Christophe Godin, and Jan Traas. Physical models of plant development. *Annual Review of Cell and Developmental Biology*, 30:59–78, 2014.

[26] Maya Bar and Naomi Ori. Leaf development and morphogenesis. *Development*, 141(22):4219–4230, 2014.

[27] Jean Philibert. One and a half century of diffusion: Fick, einstein before and beyond. 2006.

[28] Tobias Neckel. An Introduction to Finite Element Methods . https://www5.in.tum.de/lehre/vorlesungen/sci_comp/ws14/pde_fem.pdf, 2014. [Online].

[29] Hugo Hofhuis, Derek Moulton, Thomas Lessinnes, Anne-Lise Routier-Kierzkowska, Richard J. Bomphrey, Gabriella Mosca, Hagen Reinhardt, Penny Sarchet, Xiangchao Gan, Miltos Tsiantis, Yiannis Ventikos, Simon Walker, Alain Goriely, Richard Smith, and Angela Hay. Morphomechanical innovation drives explosive seed dispersal. *Cell*, 166(1):222–233, 2016.

[30] Gabriella Mosca, Milad Adibi, Soeren Strauss, Adam Runions, Aleksandra Sapala, and Richard S. Smith. *Modeling Plant Tissue Growth and Cell Division*, pages 107–138. Springer International Publishing, Cham, 2018.

[31] O. Trnka, M. Hartman, and K. Svoboda. An alternative semi-implicit euler method for the integration of highly stiff nonlinear differential equations. *Computers & Chemical Engineering*, 21(3):277–282, 1997.

[32] Erika E. Kuchen, Samantha Fox, Pierre Barbier de Reuille, Richard Kennaway, Sandra Bensmihen, Jerome Avondo, Grant M. Calder, Paul Southam, Sarah Robinson, Andrew Bangham, and Enrico Coen. Generation of leaf shape through early patterns of growth and tissue polarity. *Science*, 335(6072):1092–1096, 2012.

[33] William T. Vetterling William H. Press, Saul A. Teukolsky and Brian P. Flannery. Numerical Recipes. The Art of Scientific Computing . http://numerical.recipes/book/book.html, 2007. [Online].

[34] María Cecilia Rivara and Gabriel Iribarren. The 4-triangles longest-side partition of triangles and linear refinement algorithms. *Math. Comput.*, 65:1485–1502, 1996.

[35] Marshall Bern and David Eppstein. Mesh generation and optimal triangulation. 02 1970.

[36] Thomas M. Liebling and Lionel Pournin. Voronoi Diagrams and Delaunay Triangulations: . https://www.math.uni-bielefeld.de/documenta/vol-ismp/60_liebling-thomas.pdf, 2010. [Online].

[37] G W Lucas. An Introduction to the Delaunay Triangulation . https://gwlucastrig.github.io/TinfourDocs/DelaunayIntro/index.html, 2019. [Online].

[38] Samantha Fox, Paul Southam, Florent Pantin, Richard Kennaway, Sarah Robinson, Giulia Castorina, Yara E. Sánchez-Corrales, Robert Sablowski, Jordi Chan, Verônica Grieneisen, Athanasius F. M. Marée, J. Andrew Bangham, and Enrico Coen. Spatiotemporal coordination of cell division and growth during organ morphogenesis. *PLOS Biology*, 16(11):1–48, 11 2018.

[39] Zhongjuan Zhang, Adam Runions, Remco A. Mentink, Daniel Kierzkowski, Michal Karady, Babak Hashemi, Peter Huijser, Sören Strauss, Xiangchao Gan, Karin Ljung, and Miltos Tsiantis. A wox/auxin biosynthesis module controls growth to shape leaf form. *Current Biology*, 30(24):4857–4868.e6, 2020.